ERDC/CRREL TR-08-6

Cold Regions Research
and Engineering Laboratory

US Army Corps
of Engineers®
Engineer Research and
Development Center

Construction and Instrumentation of Full-Scale Geogrid Reinforced Pavement Test Sections

Karen S. Henry, Edel R. Cortez, Lawrence S. Danyluk,
Gregory Brentrup, Nathan Lamie, and Troy W. Arnold

April 2008

Approved for public release; distribution is unlimited.

ERDC/CRREL TR-08-6
April 2008

Construction and Instrumentation of Full-Scale Geogrid Reinforced Pavement Test Sections

Karen S. Henry, Edel R. Cortez, Lawrence S. Danyluk, Gregory Brentrup, Nathan Lamie, and Troy W. Arnold

Cold Regions Research and Engineering Laboratory
U.S. Army Engineer Research and Development Center
72 Lyme Road
Hanover, NH 03755-1290

Approved for public release; distribution is unlimited.

Prepared for F.H.W.A. Pooled Fund Study, TPF 5-010, Structural Improvement of Flexible Pavements Using Geosynthetics for Base Course Reinforcements

Abstract: A study is being conducted on full-scale pavement test sections to assess geogrid base reinforcement in flexible pavements representative of major highways. This report documents the construction and instrumentation of those test sections. The design of the test sections was based on a pavement design life of 3×10^6 equivalent single axle loads. There are two asphalt concrete and two base course thicknesses. One test section at each asphalt and base thickness was constructed with geogrid reinforcement and one without geogrid. The geogrid is located at the base course/subgrade interface. Test sections are instrumented to measure stress, strain, moisture, and temperature. They were constructed in the Frost Effects Research Facility with moisture and temperature control. The subgrade soil is AASHTO A-4 (USCS ML), and the as-built subgrade modulus values, determined by falling weight deflectometer, ranged from approximately 55.2 to 75.8 MPa (8-11 ksi). A concrete floor (simulating natural bedrock) is 2.44 m (8 ft) below the pavement surface. Analyses of results generated by this project will provide evaluation of geogrid reinforcement and will serve as the basis for the development of pavement models compatible with NCHRP 1-37A, Guide for Mechanistic-Empirical Design of New and Rehabilitated Pavement Structures (available from http://www.trb.org/mepdg/).

DISCLAIMER: The contents of this report are not to be used for advertising, publication, or promotional purposes. Citation of trade names does not constitute an official endorsement or approval of the use of such commercial products. All product names and trademarks cited are the property of their respective owners. The findings of this report are not to be construed as an official Department of the Army position unless so designated by other authorized documents.

DESTROY THIS REPORT WHEN NO LONGER NEEDED. DO NOT RETURN IT TO THE ORIGINATOR.

Contents

Figures and Tables

Figures

Tables

Preface

This report was prepared by Karen S. Henry, Edel R. Cortez, and Lawrence S. Danyluk, all of the Force Projection and Sustainment Branch; Gregory Brentrup (student employee); and Nathan Lamie and Troy W. Arnold of the Engineering Services Branch, Cold Regions Research and Engineering Laboratory (CRREL), U.S. Army Engineer Research and Development Center (ERDC), Hanover, NH.

The authors acknowledge the sponsorship by the Federal Highway Administration (FHWA) and the participating state transportation agencies. In particular, the leadership and encouragement of the Maine Department of Transportation is greatly appreciated. The authors express special gratitude to Dr. Dana Humphrey and Dr. William Davids of the University of Maine and Dale Peabody from the Maine Department of Transportation for their advice throughout the construction phase of this project.

The report was prepared under the general supervision of Dr. Jon Zufelt, Acting Chief, Force Projection and Sustainment Branch; Dr. Justin Berman, Chief, Research and Engineering Division; Dr. Lance Hansen, Acting Deputy Director; and Dr. Robert E. Davis, Director, CRREL.

The Commander and Executive Director of ERDC is COL Richard B. Jenkins. The Director is Dr. James R. Houston.

1 Introduction

The use of geogrids for reinforcement of pavements to increase their structural capacity and/or their service life has been reported in the literature indicating varying degrees of success. Generally, the reported applications and experiments have been of limited scope, and most previous research has involved thin asphalt concrete, thin or moderate base course thickness, and soft subgrades (California Bearing Ratio values of 3 or less)—e.g., the summary of 15 years of geosynthetic-reinforced base research provided by Perkins and Ismeik (1997), Vischer (2003), and Perkins and Cortez (2005). In one study, Perkins (1999) found that geosynthetic reinforcement of test sections with 75 mm (3 in.) of asphalt overlying 200–375 mm (8–14.5 in.) of base provided significant benefit when the subgrade had a CBR of 1.5 but no improvement when the subgrade had a CBR of 20.

The U.S. Federal Highway Administration (FHWA), pooled-fund study, TPF-5(010), entitled *Structural Improvement of Flexible Pavements Using Geosynthetics for Base Course Reinforcements*, with participation of nine state transportation agencies, the University of Maine, and the U.S. Army Engineer Research and Development Center's Cold Regions Research and Engineering Laboratory (ERDC-CRREL) was organized to assess the potential benefits of geogrid base course reinforcement in flexible pavements more representative of state highways than most previous work—that is, stiffer subgrades and more representative base and asphalt layer thicknesses.

Purpose and Scope of the Research Project

The purpose of this pooled-fund study is to provide data required to help determine whether geosynthetic-base reinforcement is beneficial at conditions and pavement structures typical of state highways. Pavement layer stresses and strains are being measured as a function of traffic loading in order to conform with requirements for modifications to the NCHRP 1-37A, *Mechanistic-Empirical Design of New and Rehabilitated Pavement Structures* (http://www.trb.org/mepdg/) (NCHRP 2004).

The overall objectives of TPF-5(010) were:

- To determine whether and under what conditions geosynthetics (geogrids and geotextiles) used to reinforce the base layer increase the structural capacity of pavements typically constructed by state DOTs.
- To determine whether and under what conditions geosynthetics increase the service life of pavements typically constructed by state DOTs.
- To measure in situ stress and strain responses of full-scale pavement sections so that the data are available for use in current and future pavement design processes.

The original research proposal, for a total of over $2.3 million, called for four phases of research on full-scale test sections constructed for research to be trafficked to failure with a heavy vehicle simulator (HVS). The phases described were:

- Geogrid used in test sections with a constant subgrade moisture content and modulus.
- Geogrid used in test sections with varied subgrade moisture contents caused by freezing and thawing.
- Geotextile used in test sections with a constant subgrade moisture content and modulus.
- Effect of subgrade modulus values on sections reinforced with geogrid and geotextile.

Resources acquired to date are supporting only Phase 1, and the construction of the test sections for this phase is the subject of this report. Phase 1 tests are on test sections overlying a relatively soft subgrade (resilient modulus of 34.5 MPa, or 5 ksi) with a constant moisture content.

This Phase 1 effort also includes the development of a three-dimensional finite element model that simulates the response of flexible pavements to traffic loading with and without geogrid reinforcement. Hence, the results generated in early large-scale testing by the loading with the HVS were used to help calibrate the finite element model described in Clapp (2007).

Experimental Design

To simulate traffic conditions of a typical highway, the experimental design was based on a pavement design life of 3×10^6 equivalent single-axle loads (ESALs). Based on the 1993 AASHTO design guide (AASHTO 1993) for a subgrade with a resilient modulus of 34.5 MPa (5 ksi), 610 mm

(24 in.) of base and 152 mm (6 in.) of asphalt are required. The experimental design for this project included two asphalt concrete thicknesses and two base course thicknesses (Table 1). There were eight test sections, making a 2^3 factorial design, allowing for systematic comparison of the influences of base thickness, asphalt thickness, and geogrid presence. Hence, both asphalt and base course savings by utilizing geogrid reinforcement were considered.

Table 1. Test sections for geogrid reinforced pavement.

Constructed test section number	Asphalt thickness (mm; in.)	Base thickness (mm; in.)	Geogrid between base and subgrade
1	152; 6	305; 12	no
2	102; 4	305; 12	no
3	152; 6	305; 12	yes
4	102; 4	305; 12	yes
5	152; 6	610; 24	no
6	102; 4	610; 24	no
7	152; 6	610; 24	yes
8	102; 4	610; 24	yes

Overview of Heavy Vehicle Simulator and Traffic Application

The machine used to provide traffic loading, the Mark IV heavy vehicle simulator (HVS), was manufactured by Dynatest, Inc. The HVS is 23 m (75 ft) long, 3.7 m (12 ft) wide, and 4.1 m (13. 5 ft) high and weighs approximately 50,000 kg (110,000 lb). The load on a dual-tire assembly can range from 20 to 102 kN (4.5 to 23 kips). Traffic can be uni-directional or bi-directional, and the wheel speed is a maximum 13 km/hr (8 mph). Traffic wander can be uniform or variable. The HVS can apply a range of heavy loads.

Dual truck tires are being utilized in this project, with each traffic load beginning with a 48.9-kN (11-kip) wheel load (representing a 97.8-kN, or 22-kip, axle load—the maximum that is allowed by several states). The operating pressure of the wheel is 689.5 kPa (100 psi). Traffic is applied in one direction at 12.9 km/hr (8 mph) and is allowed to wander over the 0.92-m width in the test window of each test section. The test window is the central portion of each test section to which the wheel load is applied.

At several times during the trafficking of each test section, trafficking is suspended, the wheel load is applied directly over stacks of sensors that indicate vertical deformation, and data are recorded. Thus, the total deformation occurring in the asphalt, base, and subgrade is determined. These tests are referred to as static tests.

Overview of Test Section Construction

The test sections were constructed in the Frost Effects Research Facility (FERF) of the U.S. Army Engineer Research and Development Center's Cold Regions Research and Engineering Laboratory (ERDC-CRREL) in Hanover, New Hampshire. The FERF maintains moisture and temperature conditions during construction and traffic testing. The temperature inside the FERF was kept at approximately 23°C (73°F) during construction.

The structure of the test sections included an asphalt concrete layer over a crushed stone base course over a subgrade soil, AASHTO A-4 (USCS type ML). The concrete floor was 2.44 m (8 ft) below the pavement surface. The bottom layers of the subgrade were already present in the test basin, and the top portion of the subgrade was placed and compacted beginning at a depth of 1.52 m (5 ft) down from the asphalt surface. The geogrid used in these experiments is located at the interface between the subgrade and the base. The test sections were instrumented with sensors to measure stress, strain, moisture, and temperature at strategic locations within the pavements.

Final constructed subgrade modulus values, measured by a falling-weight deflectometer (FWD), of approximately 55.2–75.8 MPa (8–11 ksi), were achieved by constructing the subgrade of the test sections at near optimum moisture content and maximum dry density and subsequently adding water to the test basin near the top of the subgrade, which resulted in a lowering of the modulus. The process used to lower the subgrade modulus took about five months. During this time water was added in increments, and periodic monitoring with FWD tests was performed in coordination with moisture content readings.

Purpose and Scope of this Report

This report documents, in detail, the construction and instrumentation of the test sections. As reports containing performance data are subsequently published, the construction details will be important for data interpretation and analyses.

2 Description of the Test Sections

The test sections were constructed in a test basin that is 6.4 m (21 ft) wide with concrete walls and a floor at 2.44 m (8 ft) from the pavement surface (Fig. 1). Figure 2 shows cross sections of the test basin for Test Sections 3, 4, 7, and 8. The thickness of the base course is 0.30 m (1 ft) for Test Sections 1–4 and 0.61 m (2 ft) for Test Sections 5–8. The asphalt thickness for the east lane (Test Sections 2, 4, 6, and 8) is 102 mm (4 in.). The asphalt thickness for the west lane (Test Sections 1, 3, 5, and 7) is 152 mm (6 in.).

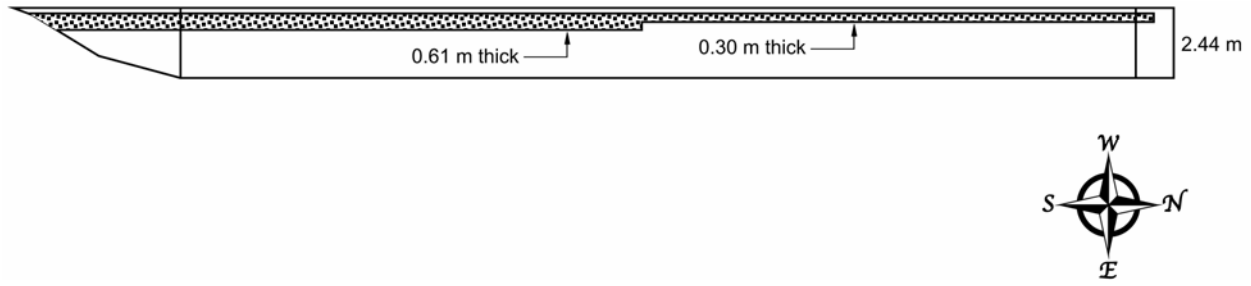

a. Longitudinal cross-section view of a test basin showing the two base course thickness.

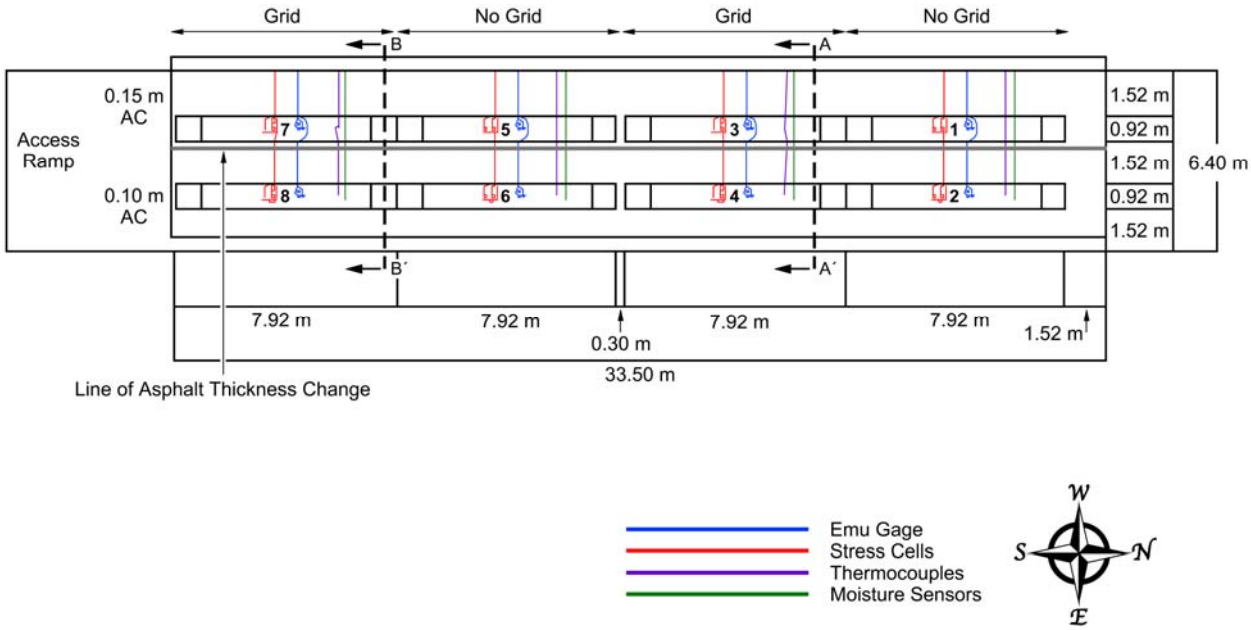

b. Plan view, indicating test windows (the long, numbered rectangles, where traffic was applied) and instrumentation.

Figure 1. Layout of the test basin.

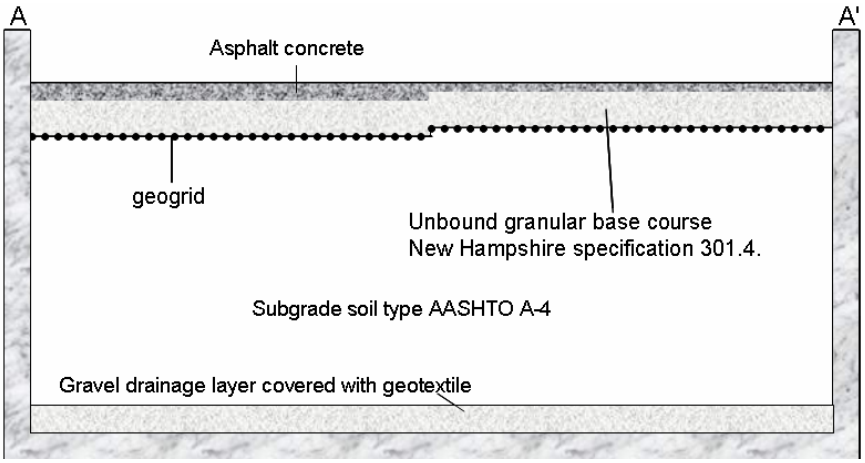

a. Test Sections 3 and 4, corresponding to A-A' on Figure 1b (not to scale).

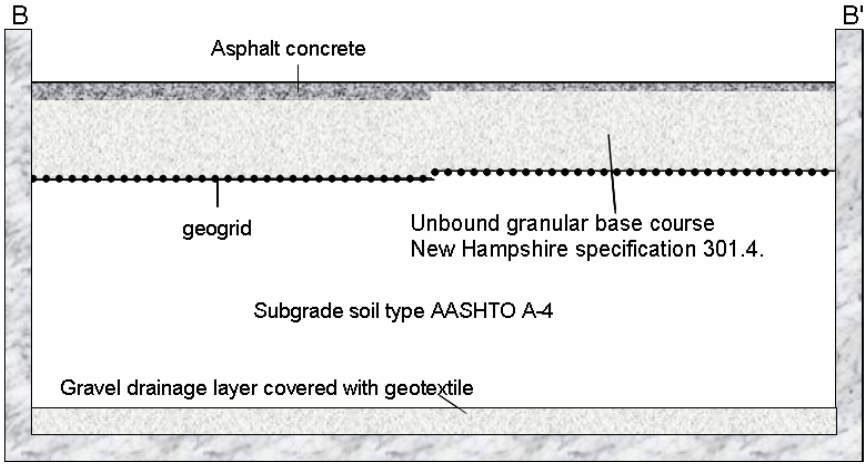

b. Test Sections 7 and 8, corresponding to B-B' on Figure 1b (not to scale).

Figure 2. Cross sections of two test sections.

The subgrade thickness is either approximately 1.5 m (5 ft) or 1.8 m (6 ft). For the previous research project, the test basin had been lined with an impermeable membrane to prevent drainage, and a 254-mm (10-in.) layer of gravel had been placed in the bottom of the test basin (below the subgrade) to facilitate moisture control. The layer of gravel (drainage layer) is separated from the overlying subgrade by a needle-punched geotextile. The bottom gravel layer was used to promote the uniform distribution of water below the subgrade layer for moistening the subgrade. For this project, the geomembrane liner was removed from the side walls to a depth of 1.5 m (5 ft) from the asphalt surface and was left in place below that depth.

The test window, or the portion of the test section to which the wheel load is applied on the surface, is 0.91 m (3 ft) wide by 7.9 m (26 ft) long, with

0.91-m (3-ft) transition zones on each end (Fig. 1 and 3). The transition zones are where the wheel load is applied and accelerated (on the north side) and decelerated and removed (on the south side), so that the central 6.0 m (20 ft) of the test window are trafficked at constant load and speed. The coordinate system utilized to document the location of sensors within the test windows that is used in Appendix A (as well as marked on each test section) has the origin (0,0,0) located at the surface of the asphalt and at the center of the test window of each test section, as shown in Figure 4.

Figure 3. Paved test sections showing test windows (outlined in yellow) to which traffic was applied, including the short transition sections. Traffic was applied in a direction away from the viewer of this image.

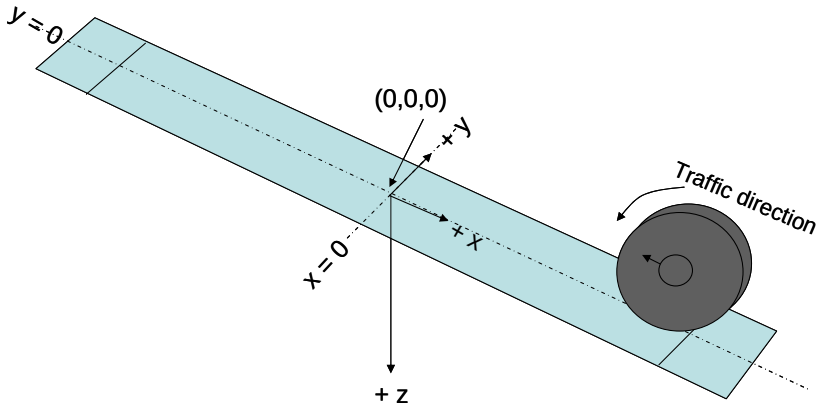

Figure 4. Local coordinate system for each test window. The traffic direction was from north to south.

3 Material Properties

The subgrade, Hanover silt, is native to the Connecticut River valley in the local Hanover, NH, area. The base is unbound crushed stone obtained from a quarry in Lebanon, NH. The source rock is an amphibolite. It is classified as AASHTO A-1 (USCS type GP-GM, a mix of poorly graded gravel and silty gravel). The fines are non-plastic. The base meets New Hampshire specification 301.4 for base course materials. The test soils' grain size distributions, soil classification information, and compaction curves (modified Proctor) are presented in Table 2 and Figures 5–7. Figure 6 also shows California bearing ratio determinations for the subgrade soil as a function of soil moisture.

Table 2. Soil properties. Dry density and optimum moisture content were determined according to AASHTO T-180 (modified Proctor).

Property	Subgrade	Base
AASHTO	A-4	A-1
USCS	ML	GP-GM
Specific Gravity	2.72	2.7
LL (%)	28	Not applicable, fines non-plastic
PI	8	Not applicable, fines non-plastic
Optimum moisture content (%)	13.3	5
Maximum dry density (kg/m^3; pcf)	1922; 120	2383; 149
% passing ¾ in.	98.6	82
% passing #200	73.3	5.4

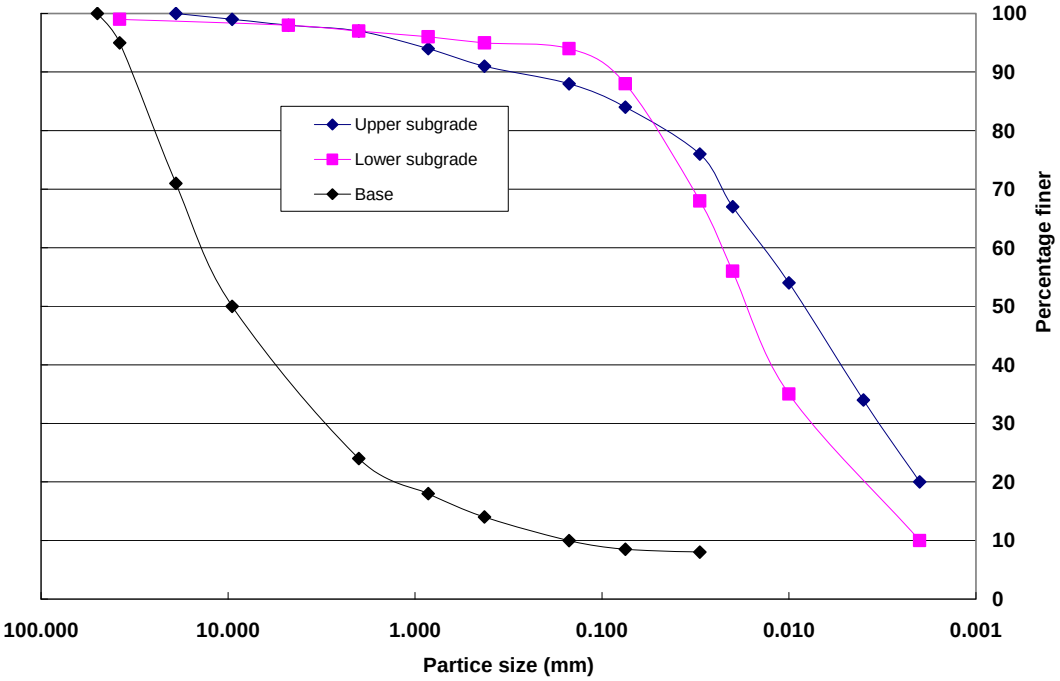

Figure 5. Grain size distribution of the subgrade and base course soils. "Upper subgrade" refers to the material that was placed beginning at a depth of 1.52 m (5 ft) from the top of the asphalt, while "Lower subgrade" refers to soil that was already in place at the time of construction.

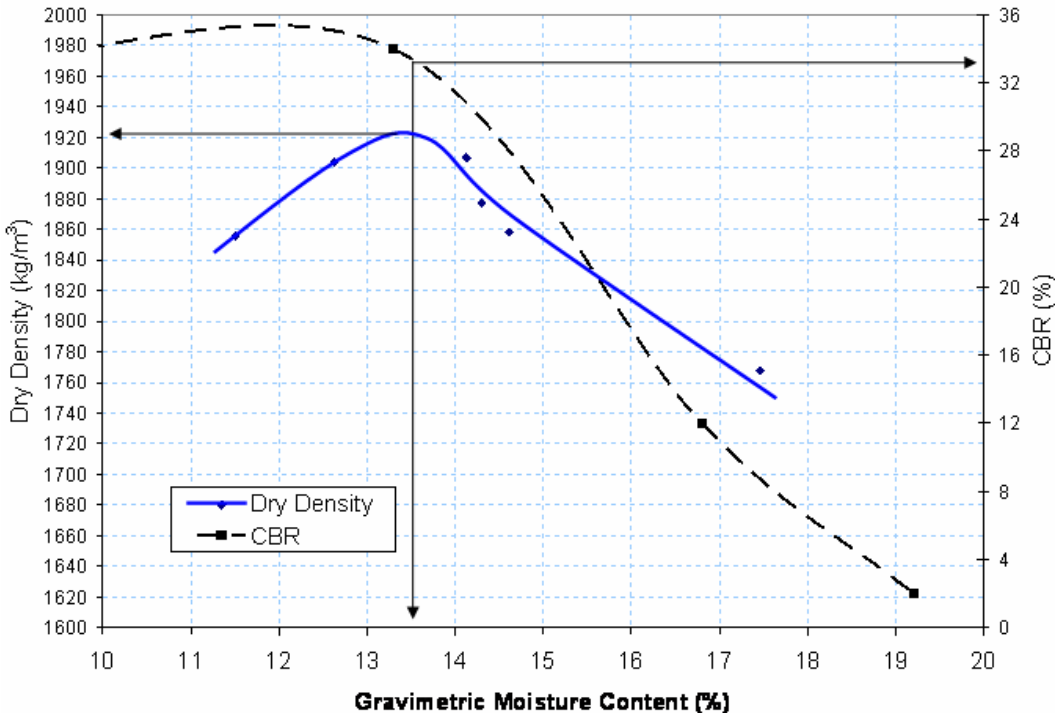

Figure 6. Modified Proctor and laboratory CBR test results for the subgrade soil.

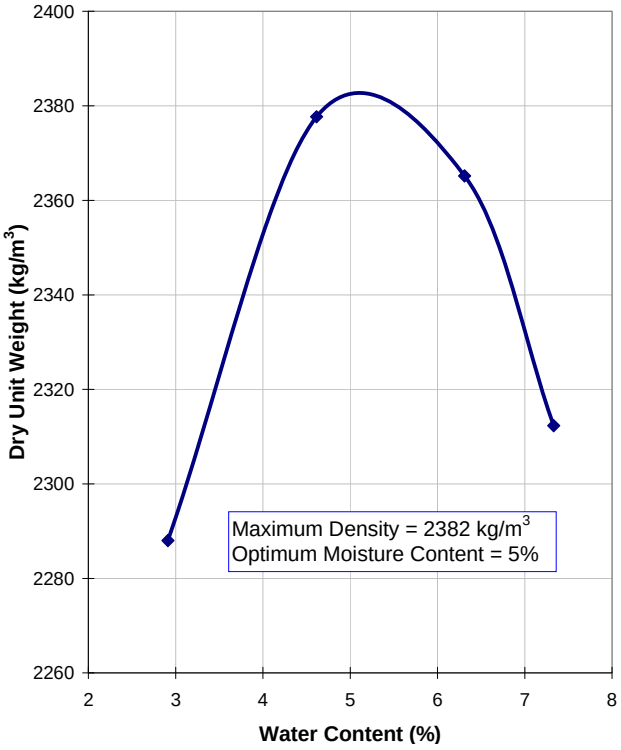

Figure 7. Modified Proctor test results for the base course. The maximum dry density is 2383 kg/m³ and the optimum moisture content is 5%.

Laboratory determinations of resilient modulus were made for the subgrade and base using AASHTO Standard T-307-99, *Determining the Resilient Modulus of Soil and Aggregate Materials*. Due to the low plasticity of both soils, in situ sampling was not practical. The resilient modulus subgrade specimens were compacted by hand at optimum water content to the maximum dry density in six lifts. Each layer was scarified on the top to promote a uniform structure. Specimens were 152 mm (6 in.) high by 71 mm (2.8 in.) in diameter. The base specimen was 305 mm (12 in.) high by 152 mm (6 in.) in diameter and was compacted by pouring the aggregate into the mold and tapping it to promote densification. Neither specimen preparation procedure is specified in AASHTO Standard T-307-99; however, they did produce the densities required to simulate the soil compaction.

The stress conditions used in the tests represent the range of stress states that occur in pavements due to traffic loading. The results of the subgrade and base resilient modulus determinations are summarized in Tables 3 and 4.

Table 3. Resilient modulus values for four compacted subgrade specimens—three compacted at maximum dry density and optimum moisture content, one compacted at maximum dry density then subsequently saturated prior to testing.

Specimen	Water content (%) (gravimetric)	Dry density (Mg/m^3; lb/ft^3)	Confining pressure (kPa)	Peak cyclic stress (kPa)	Resilient modulus	
					(MPa)	(psi)
15-4	13.1	1.827; 114.0	13.8	24.6	77	11,170
			13.8	37.3	72	10,440
			13.8	49.1	71	10,300
			13.8	61.6	73	10,590
			27.6	24.5	93	13,490
			27.6	36.9	88	12,760
			27.6	49.6	83	12,040
			27.6	61.4	82	11,890
			41.4	25.1	116	16,820
			41.4	49.5	97	14,070
			41.4	61.6	93	13,490
15-3	13.1	1.840; 114.4	13.8	24.5	110	15,950
			13.8	37	86	12,470
			13.8	49.1	81	11,750
			13.8	61.6	81	11,750
			27.6	24.5	124	17,990
			27.6	36.5	105	15,230
			27.6	49	102	14,790
			27.6	61.7	94	13,630
			41.4	24.9	139	20,160
			41.4	36.9	117	16,970
			41.4	49.1	115	16,680
			41.4	61.9	110	15,950
15-2	13	1.840; 114.4	13.8	24.4	138	20,020
			13.8	37.4	91	13,200
			13.8	49.5	84	12,180
			13.8	61.7	87	12,620
			27.6	24.5	103	14,940
			27.6	37.7	83	12,040
			27.6	49.6	85	12,330
			27.6	61.5	82	11,890
			41.4	37	97	14,070
			41.4	49.7	92	13,340
			41.4	62	90	13,050
GeoSat-1 (saturated)	Initial – 13.0 Final – 21.6	(1.74; 108.7)	13.8	27.6	25	3,650
			13.8	41.2	25	3,630
			13.8	55.5	30	4,420
			13.8	68.7	33	4,760
			27.6	28.1	31	4,510
			27.6	41.3	31	4,470
			27.6	54.8	32	4,570
			27.6	68.7	33	4,840
			41.4	28.0	32	4,680
			41.4	41.9	47	6,830
			41.4	55.7	42	6,150
			41.4	69.7	38	5,550

Table 4. Resilient modulus values for a base layer specimen compacted at optimum water content to maximum dry density.

Water content (%) gravimetric	Dry density (Mg/m^3; lb/ft^3)	Confining pressure (kPa)	Peak cyclic stress (kPa)	Resilient modulus	
				(MPa)	(psi)
2.9	2.258; 141.0	34.5	30.8	155	22,481
		34.5	60.8	224	32,488
		34.5	92.1	237	34,373
		69.0	62.2	265	38,435
		69.0	123.0	291	42,205
		69.0	186.0	334	48,442
		103.5	59.5	348	50,473
		103.5	91.5	352	51,053
		103.5	185.8	415	60,190
		137.9	92.1	396	57,434
		137.9	123.9	504	73,099
		137.9	245.2	451	65,412

The laboratory-measured resilient modulus values for the saturated subgrade were approximately 30–60% of the values of the subgrade compacted at optimum water content. Further, they were the desired test values for trafficking. Hence, the stiffness of the constructed subgrade was lowered by adding water as described later in this report.

The geogrid used in these experiments, Tensar BX1200, was chosen because it has been used in similar studies in the past, and it is relatively easy to instrument with strain gages (Fig. 8). This allows comparison between test results generated by this study and others reported in the literature.* The mechanical properties provided by the manufacturer for the geogrid are listed in Table 5. Additional information can be found at the following link: http://www.tensarcorp.com/uploadedFiles/SPECTRA_MPDS_BX_10.07.pdf.

* The selection of this particular geogrid does not imply endorsement of it.

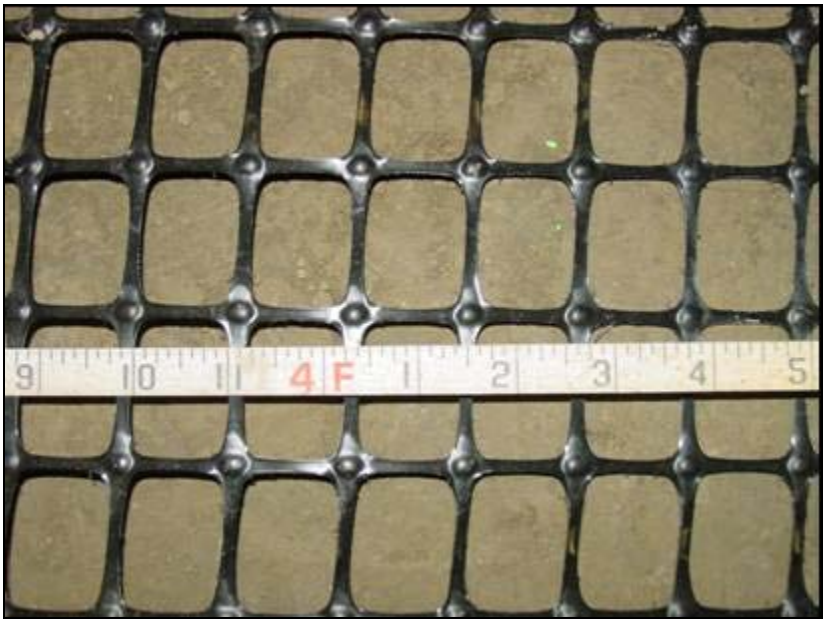

Figure 8. Tensar® BX1200 geogrid.

Table 5. Properties of geogrid used in the test sections.

Aperture size (mm; in.)		Wide-width tensile strength at 2% strain* (kN/m; lb/ft)	
Machine direction	Cross-machine direction	Machine direction	Cross-machine direction
25; 1.0	33; 1.3	6.0; 410	9.0; 620

*Determined according to ASTM D6637.

The hot mixed asphalt (HMA) material conformed to the New Hampshire specifications for a Type B base course and Type F surface course. Type B gradation requires that 95–100% of the aggregates pass the 19-mm (0.75-in.) sieve. The Type F requires that 95–100% pass the 9.5-mm (0.375-in.) sieve size. The gradations and ranges of asphalt content for both mixes are presented in Table 6, and measured gradations provided by the Maine DOT based on tests of an asphalt core are provided in Table 7. Tests on the asphalt cores also indicated that the asphalt aggregate had a bulk specific gravity of 2.6 and an average air void content of 2.1%.

The asphalt binder grade was PG 64-28. This asphalt grade is commonly used for highway construction by paving contractors in the Hanover, New Hampshire, area.

Table 6. NHDOT asphalt concrete gradation and asphalt content ranges.

Sieve size	Type B – base course, percentage passing			Type F – surface course, percentage passing		
	Min	Desired	Max	Min	Desired	Max
31.8 mm (1.25 in.)						
25.4 mm (1 in.)						
19.1 mm (0.75 in.)	95	100	100			
12.2 mm (0.5 in.)	70	81	92			
9.5 mm (0.375 in.)	60	71	80	95	100	100
4.75 mm (No. 4)	42	50	57	64	71	80
2.00 mm (No. 10)	28	32	38	44	50	55
0.85 mm (No. 20)	16	20	24	25	30	35
0.425 mm (No. 40)	9	13	17	15	20	25
0.180 mm (No. 80)	3	7	11	6	11	16
0.075 mm (No. 200)	0	3	4	2	4	6
% Asphalt Content*	4.8	5.25	6.0	6.25	6.5	7.0

*The asphalt content is based on the use of aggregates with a specific gravity of 2.65 to 2.70.

Table 7. Asphalt concrete gradation measured on asphalt cores taken after paving. (There was no distinction between base and surface course.)

Sieve size	Percentage passing
31.8 mm (1.25 in.)	
25.4 mm (1 in.)	100
19.1 mm (0.75 in.)	98
12.2 mm (0.5 in.)	92
9.5 mm (0.375 in.)	85
4.75 mm (No. 4)	57
2.36 mm (No. 8)	43
0.60 mm (No. 30)	23
0.35 mm (No. 50)	14
0.152 mm (No. 100)	8
0.075 mm (No. 200)	5
% Asphalt Content	5.8

4 Instrumentation

Each test section was instrumented with moisture and temperature sensors, triaxial strain gages (εmu coils), and pressure cells. Figure 9 shows a typical plan view and cross section of the portion of a geogrid test section in which instrumentation was installed. The locations of all the sensors are documented in detail in Appendix A. In addition to the installed coils, a hand-held εmu coil is placed over the asphalt surface to measure the vertical deformation of the asphalt layer when deformation readings are made. Additional details about each sensor are provided below.

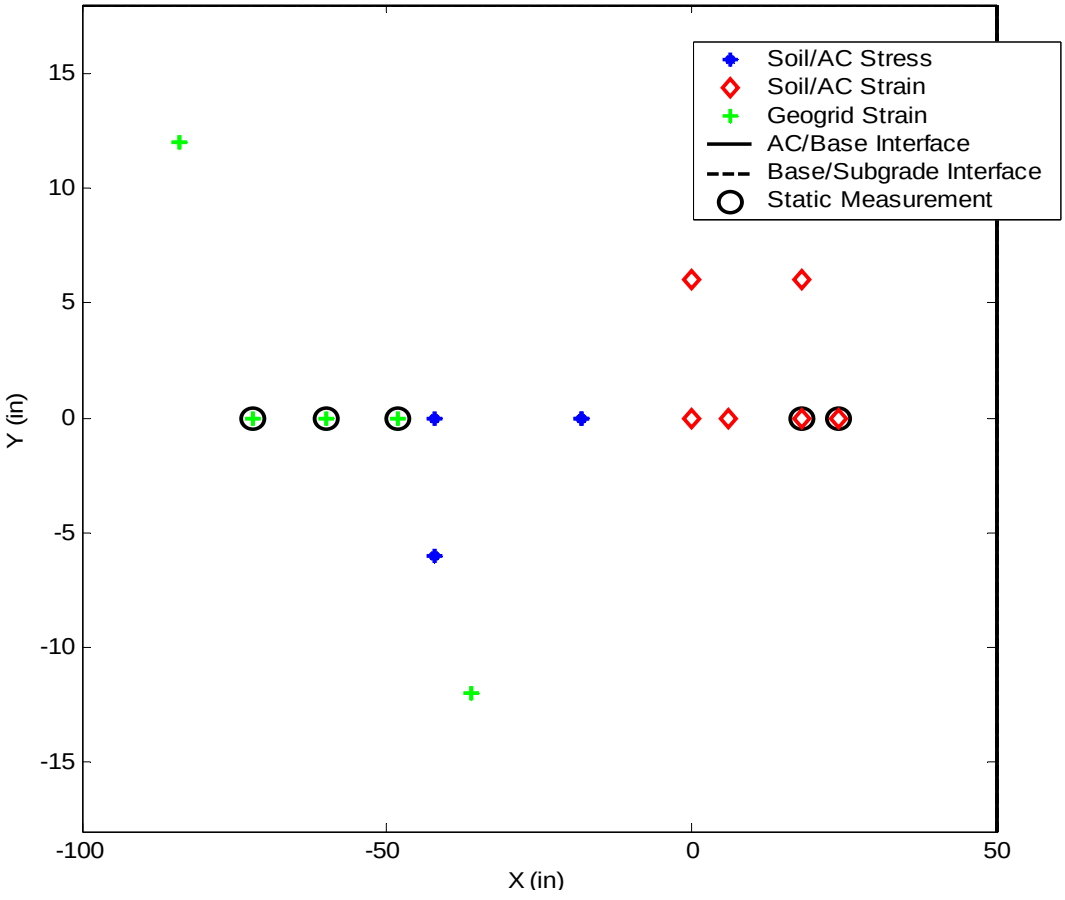

a. Plan view.

Figure 9. Locations of instrumentation of a geogrid test section. The locations of static load tests are also shown.

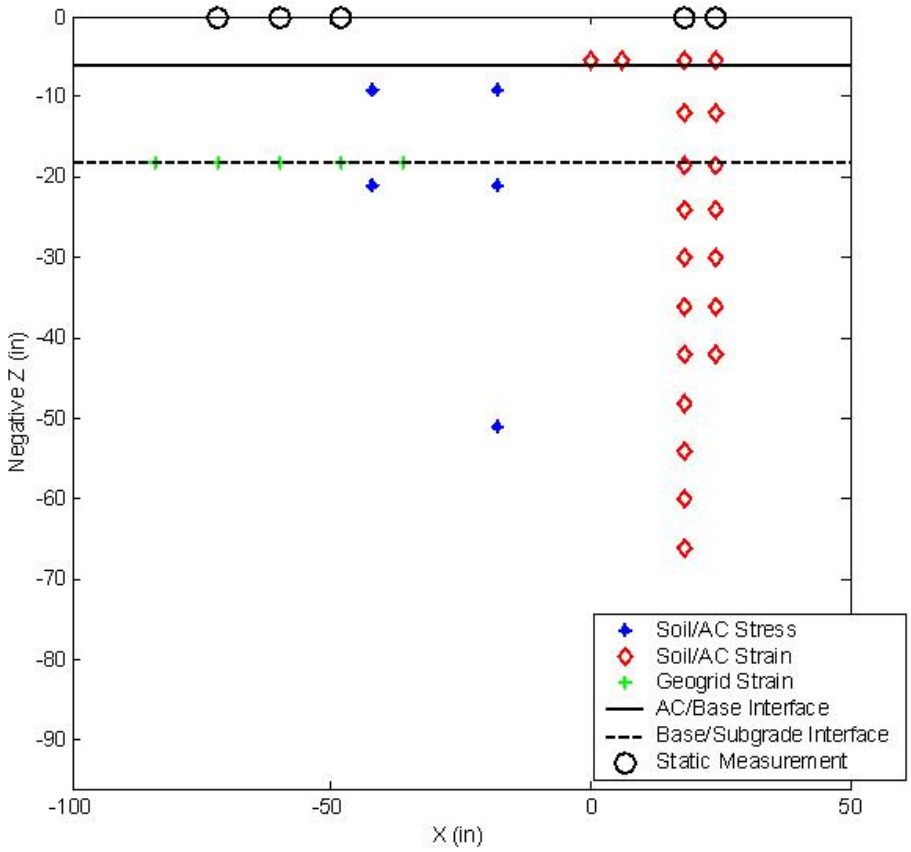

b. Cross section.

Figure 9 (cont.). Locations of instrumentation of a geogrid test section. The locations of static load tests are also shown.

Temperature Sensors

Copper-constantan, Type T thermocouples were installed to measure temperatures in the asphalt and soil layers. The accuracy of these thermocouple measurements is ±0.5°C. (The Type T thermocouples are measured differentially at a range of ±2.5 mV, which yields a resolution of 0.33 μV.) Temperatures are recorded by Campbell Scientific CR10X dataloggers (described below), which have internal thermistors that provide a reference temperature. The dataloggers were programmed to record temperature and moisture measurements every four hours.

Moisture Sensors

ECH$_2$O™ soil moisture sensors (Echo probes), model EC-20 (200 mm long), were installed to record volumetric soil moisture content in the base course and subgrade (Fig. 10). Echo probes measure the dielectric constant of the surrounding soil by finding the rate of change of voltage on a

sensor embedded in the soil. The relative permittivity (i.e., dielectric constant) is approximately 80 for water, 4 for most rock-forming minerals, and 1 for air. This high value for water results in relatively large changes in the permittivity of soil when the water content changes. The accuracy of an EC-20 probes in medium-textured soil types is typically ±4%, and the resolution is 0.1%. (The Echo soil moisture probes are measured differentially at the ±2500-mV range. At that range the resolution of the measurement is 333 μV.)

Figure 10. Echo soil moisture sensor.

Pressure Cells to Measure Stress

Geokon® soil pressure cells were installed in the base course and subgrade of each test section for the purpose of measuring soil stress (Fig. 11). The pressure cells consist of two circular stainless steel plates welded together around the periphery and enclosing a fluid connected to a pressure transducer through a high-pressure stainless steel tube. The pressure transducer outputs a voltage that is calibrated to produce a stress measurement.

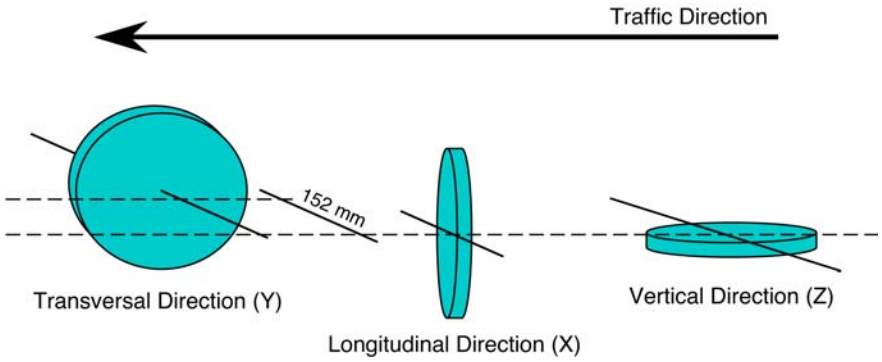

Figure 11. Orientation of pressure cells.

The pressure cells were installed in three perpendicular directions—vertical, longitudinal (in the direction of traffic), and transverse (perpendicular to the direction of traffice). The pressure cells in the transverse direction were offset 152 mm (6 in.) to avoid measurement directly beneath the wheel load, in which case the transverse component of stress may be negligible.

Soil and Asphalt Strain Sensors

Electromagnetic induction (εmu) coils were installed to measure deformations in the vertical and horizontal directions. They can be used for static or dynamic deformation measurement; in this project, they are being used for determining permanent deformation via static measurement. They were manufactured and calibrated at ERDC-CRREL. The εmu coils do not touch each other but "float" in the soil, similar to small stones embedded in a fine soil mass.

These coils work in pairs. One coil, called the sender, is energized by an external power supply. A companion coil, the receiver, is located within the electromagnetic field of the sender and produces an induced current that is proportional to the distance between the coils. When a traffic load compresses a pavement layer, the change in inter-coil distance is detected by a change in induced voltage, which increases as the distance between coils decreases. Based on the known initial distances between coil pairs, the average strain for a layer is calculated. The εmu coils and the measurement system used in this project are the same as used in a previous project, described in detail in Janoo et al. (2003), which includes detailed calibration information. This report can be downloaded from http://www.crrel.usace.army.mil/library/technicalreports/TR03-5.pdf.

Special calibration jigs were made to determine voltage output as a function of sensor spacing. For both coplanar and coaxial calibration, the transmitting coil was fixed and the receiving coil was on a moveable frame, initially 140 mm away from the transmitting coil. After excitation, voltage measurements were made as the distances between the coils were increased in increments up 25.4 mm. The following equation gives a good fit to the data:

$$V = aD^n \tag{1}$$

where D = static distance between the transmitting and receiving devices
V = demodulated (d.c.) "static" voltage from the coils
a and n = regression coefficients for a pair of coils.

Geogrid Strain Gages

Ten electrical resistance strain gages were fastened to the geogrid in each test section to make longitudinal and transverse strain measurements on

the top and bottom of the grid. Five strain gages were fastened on the upper side of the geogrid, and five were fastened at corresponding locations on the lower side of the geogrid. The strain gages were Texas Measurements model FLA-5-23, which are capable of measuring up to 3% strain and have a gage factor of 2.16. The gages had a copper-nickel alloy foil element, 0.003–0.007 mm (0.00012–0.00027 in.) thick on a 1- × 3-mm (0.39- × 0.12-in.) epoxy backing, which was attached to the geogrid ribs using two-part epoxy. Each gage had pre-soldered lead wires that were connected to the ERDC-CRREL data acquisition system. Readings were taken by applying an excitation voltage of approximately 2500 mV. Measurements utilized a Wheatstone bridge (Fig. 12).

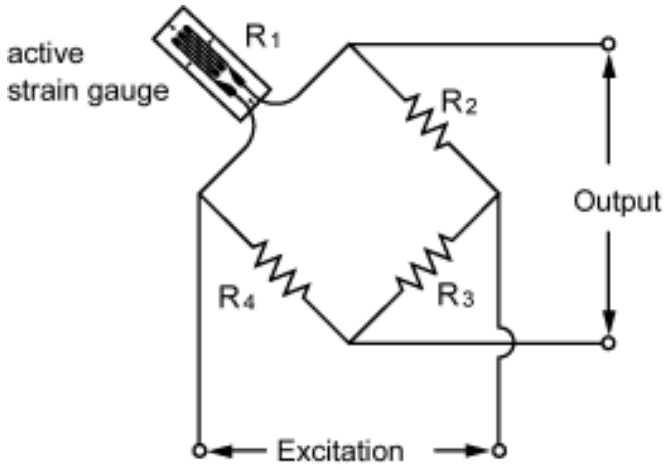

Figure 12. Wheatstone bridge configuration used for strain gage measurement. (From http://www.straingage.com/strain_gage/what_strain.php, accessed on 5 December 2007.)

For a Wheatstone bridge with a constant excitation voltage, changes in gage resistance are directly proportional to changes in the strain of the gage. The Wheatstone bridge circuit converts the resistance change into voltage output via the following equation:

$$e = \frac{R_1 R_3 - R_2 R_4}{\left(R_1 + R_2\right)\left(R_3 + R_4\right)} E \tag{2}$$

where e is the voltage output of the strain gage, E is the excitation voltage, and the R values are as defined in Figure 12. Assuming that all of the resistances (R_1 to R_4) are equal and that the change in resistance of the gage (ΔR_1) is much smaller than its unstrained resistance, this equation simplifies to:

$$\Delta e = \frac{\Delta R}{4R} E = \frac{E}{4} K\varepsilon \tag{3}$$

where K is the gage factor and ε is the strain experienced by the gage.

More information about the theory of operation can be obtained at Texas Measurements, Inc. (2008). Initial resistance readings on the strain gages verified that the strain gages were operational.

The strain gages were applied to the geogrid in the same manner as described in Helmstrom et al. (2006). The surface of the individual ribs of the geogrid, on which the strain gages were attached, were first roughened with emery cloth and then coated with Texas Measurements poly-primer. A piece of Scotch tape was applied to the gage backing, and Cyanoacrylate CN adhesive was applied to the gages. The gages were then centered on the prepared ribs and the tape held them in place while the adhesive cured. Direct pressure was applied to the gage for a minimum of one minute, and the tape was not peeled from the back of the gage until a minimum of five minutes curing time.

Data Acquisition System

All cables of the sensors embedded in the test sections were routed underground through test section "portholes" to an instrumentation tunnel located on the west side of the test sections. The cables were connected to boards on which they were organized and then routed to the appropriate data acquisition system (Fig. 13).

The data acquisition for this project consists of four subsystems. The moisture and temperature sensors are connected to a system of commercially available, Campbell Scientific CR10X dataloggers. The dataloggers are networked with a computer located in the control room of the FERF facility, which is then accessed via an internal network by researchers. The CR10X

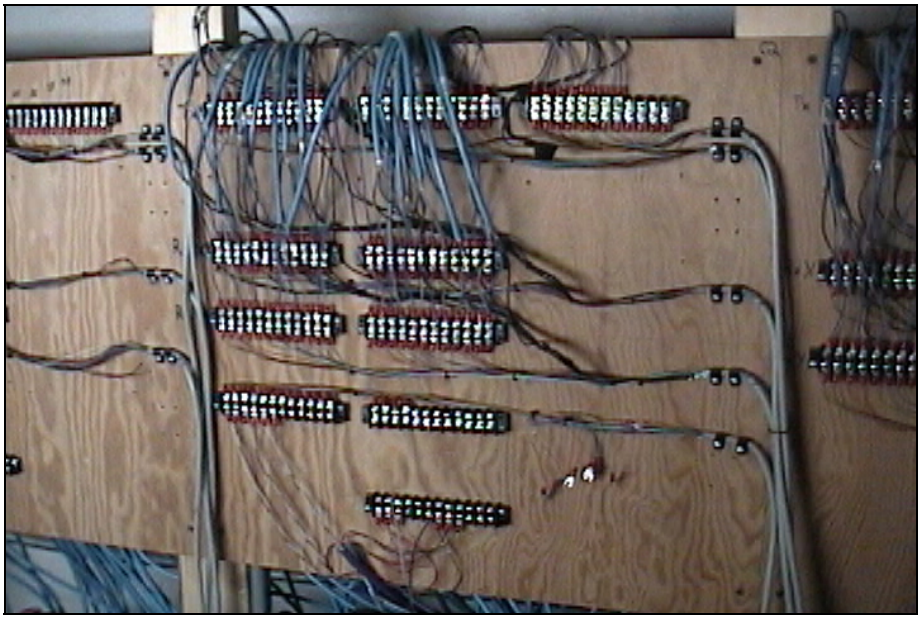

Figure 13. Cable connections on a board located in the instrumentation tunnel.

is a fully programmable datalogger/controller with non-volatile memory and a battery-backed clock. It is a small, rugged, sealed module. The CR10X has an input voltage range of ±2500 mV to ±2.5 mV. To handle the large number of sensors, three Campbell Scientific AM416 multiplexers are used. The AM416 is a multi-channel relay board with gold-clad silver alloy screw-down terminal contacts. The initial contact resistance is less than 0.1 ohms, and the switching time between relays is less than 1 ms.

A second subsystem consists of the sensors and controls within the heavy vehicle simulator. This system, an integral part of the HVS, keeps records of the number of traffic passes, traffic wander, and average load intensity for each pass. The third data acquisition subsystem is the laser profilometer, which is connected to a notebook computer that automatically logs data related to rut depth measurement whenever the profilometer is operating. The laser profilometer is commercially available from Dynatest and was developed for accurately measuring ruts developed by HVS traffic.

The fourth subsystem is a high-speed data acquisition system developed at ERDC-CRREL to collect and preprocess the signals from the stress and strain sensors. National Instruments LabVIEW is used in conjunction with an NI 6033E data acquisition card to read the outputs of the εmu coils and the strain gages. The NI 6033E has 64 single-ended analog input channels. The resolution is 16 bits, or 1 in 65,536. The maximum sampling rate is 100 kS/s. The accuracy at full scale is 1.15 mV. For data security and

reliability purposes, this computer is networked with only one other computer that, in turn, is connected to a larger internal network. The hardware and software of this data acquisition subsystem were developed by ERDC-CRREL electronic engineers because no suitable commercially available system was found at the time of its development.

5 Construction of the Test Sections

Subgrade Construction

The subgrade was placed in layers approximately 152 mm (6 in.) thick on top of soil that was already in place to a depth of 1.52 m (5 ft) below the paved surface. The subgrade soil was placed in the test basin by a front-end loader, and a bulldozer spread the soil to a grade slightly higher than the target for a given layer (Fig. 14). The soil was then cultivated with a rototiller to promote uniform moisture distribution (Fig. 15), and the moisture content of the soil was measured with a nuclear gage. The moisture deficit was established, and the amount of water needed to reach the moisture target was calculated. The required amount of water was then added in strips of 1.52 m (5 ft) across the width of the test section. The soil was cultivated again and then compacted. A smooth steel roller was used for compaction until the target density was achieved. A plate compactor was used to compact the soil near the edges of the test basin (Fig. 16). Typically, eight passes with the roller were required to achieve compaction. Once compaction was achieved, sensors were installed, a new soil lift was placed, and the process was repeated until the subgrade was completed at the planned grade.

Figure 14. Front-end loader and bulldozer that were used to build the test sections.

Figure 15. Cultivating the soil to facilitate moisture absorption and uniform distribution.

Figure 16. Plate compactor used to compact the edges of the test section.

Quality Control

Moisture and density measurements were made on each layer to ensure that it was constructed at near-optimum moisture content and maximum dry density. Measurements were made with a Troxler® 3450 nuclear density meter in the direct mode with the probe inserted 152 mm (6 in.) into the soil. Direct transmission readings were taken for one minute, which yields a precision of 2.6 kg/m^3 (0.16 lb/ft^3) and a composition error of 8.0

kg/m³ (0.50 lb/ft³) for dry density and a precision of 240 kg/m³ (15 lb/ft³) and a composition error of 5.5 kg/m³ (0.34 lb/ft³) for moisture. Appendix B contains the moisture and density measurements for each layer constructed. The average as-built subgrade moisture content was 12.2%, compared to the modified Proctor optimum moisture content of 13.3%. The average subgrade density was 1858 kg/m³ (116.0 lb/ft³), compared to the maximum modified Proctor density of 1922 kg/m³ (120.0 lb/ft³). This corresponds to 97% compaction.

For each test section, drive-cylinder specimens were obtained and ASTM D 2937, *Standard Test Method for Density of Soil in Place by the Drive-Cylinder Method*, was used to determine the in situ, dry unit weight at the top of the subgrade at the north edge of the traffic/transition window, in the middle of the traffic window, and at the south edge of the traffic/transition window (Table 8).

Table 8. Dry density measurements on the top of the subgrade, determined according to ASTM D 2937.

Test section	Dry density (kg/m³; pcf)		
	North	Middle	South
1	1907; 119.1	1940; 121.1	2027; 126.5
2	1932; 120.6	1894; 118.2	2008; 125.4
3	2044; 127.6	2028; 126.6	1912; 119.4
4	1997; 124.7	1948; 121.6	1966; 122.7
5	1925; 120.2	1832; 114.4	1829; 114.2
6	1840; 114.9	1852; 115.6	1955; 122.0
7	1896; 118.4	1908; 119.1	1859; 116.1
8	1837; 114.7	1866; 116.5	1834; 114.4

Strength Measurements made on the Subgrade Surface

Two types of measurements—using a dynamic cone penetrometer (DCP) and a Clegg impact hammer—were made on the top of the finished subgrade and were used to estimate the California bearing ratio at several points. The CBR estimates based on these readings are contained in Appendix C. The DCP test apparatus used is manufactured by Kessler Soils Engineering Products, Inc. The DCP hammer weighs 8 kg (17.6 lb). The DCP–CBR conversions were obtained using an automated Excel spreadsheet provided by the instrument manufacturer, which utilized the following empirical correlation (Webster et al. 1992):

$$CBR(\%) = \frac{292}{\left(\frac{mm}{blow}\right)^{1.12}}. \quad (4)$$

The Clegg impact hammer is essentially an AASHTO compaction hammer fitted with a piezoelectric accelerometer (Fig. 17).

Figure 17. Clegg impact hammer.

Transitions between Test Sections

To construct the test sections so that the final asphalt surface would be level at the same elevation and accommodate the differences in asphalt and base course thicknesses, adjustments were made to the elevations of the top of the subgrade. This was accomplished by using a barrier constructed of wood to compact soil against when the subgrade soil in the adjacent area of the test basin was finished at a higher elevation. The soil compacted easily, and the transitions were quite sharp, as shown in Figure 18.

Figure 18. Differences in elevation of the top of the subgrade between test sections.

Installation of Instrumentation

Prior to any soil placement, marks were made on the four sides of the test basin to indicate the depth (vertical) and horizontal locations of each sensor. As the construction progressed, wires were stretched east-west to matching locations on opposite sides of the test basin to indicate the location of the center of each sensor (Fig. 19).

Figure 19. Instrumentation installation, showing a wire extended across the test basin for precisely locating sensors.

When placing a sensor, a small amount of soil was hand-excavated from the compacted lift surface to place the sensor, and a trench was hand-excavated for the cable that connected the sensor to a datalogger located on the outside of the test basin (Fig. 20). The cables were placed into the trenches with ample slack. They were routed through the nearest of four "portholes" in the west side of the test basin (e.g., Fig. 19). Great care was taken to restore the soil density after the installation of each sensor and wire.

Figure 20. Top view of pressure cells during installation, showing trenches and cable.

During installation of the εmu coils, the surface of the soil was raked smooth and level, and, if necessary, a small amount of soil was hand-excavated so that when the coils were installed they were level and were placed at their precise x, y, z coordinates. A template was used to keep the distance between εmu coils constant and at right angles (Fig. 21). For placement of the εmu coils at the bottom of the asphalt layer, fresh asphalt concrete was excavated by hand to install the sensors at the bottom of the asphalt concrete layer (Fig. 22). Then, asphalt concrete was hand-placed on top of them, and the asphalt concrete was compacted as usual. (Asphalt paving is discussed in more detail in a subsequent section.)

Figure 21. Installation mold for placement of three εmu coils.

Figure 22. Installing εmu coils in the hot asphalt concrete.

Geogrid Installation and Placement of Base Course Layer

For the geogrid reinforced test sections, an instrumented geogrid sheet was installed over the finished subgrade so that the center of the geogrid sheet was aligned with the center of the test window (Fig. 23). Small amounts of base course material were placed over the geogrid sheet at the middle to hold it in place. The sheet was then stretched by hand and anchored by placing additional base material until the sheet was wrinkle-free, aligned, and at the intended location (Fig. 24, 25).

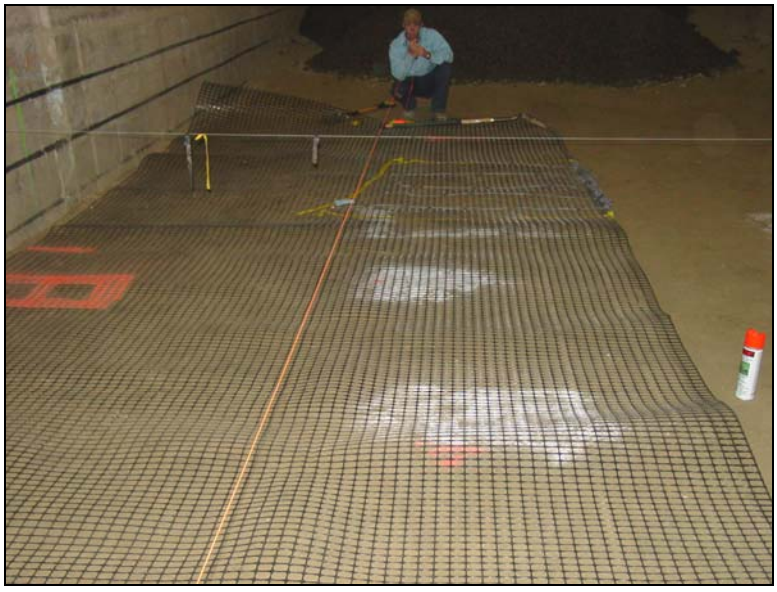

Figure 23. Alignment of instrumented geogrid with tire path. The measuring tape is in the center of the test window.

Figure 24. Geogrid partially covered with base course aggregate.

Figure 25. Close-up of geogrid and base aggregate particles.

The strain gages and their lead wires were covered with sand-size material sieved from the base course material. This was done to protect these delicate sensors from potential load concentrations caused by larger aggregate particles. The remaining base course material was placed in 152-mm (6-in.) layers, moistened and compacted until the target moisture and density were achieved. Voltage readings of the strain gages attached to the geogrid were not made before and immediately after construction (this was an oversight); however, during testing, initial deformation readings were made immediately prior to trafficking each test section with the HVS.

The base aggregate was placed in layers approximately 152 mm (6 in.) thick. It was moved to the test basin by a front-end loader, and a bulldozer tractor spread it to a grade slightly higher than the target for a given layer. It was rolled with a smooth steel roller to achieve compaction, usually requiring about eight passes. For each layer, the moisture deficit was established, and the amount of water needed to reach optimum moisture content was determined and then added to the aggregate. Although the optimum moisture content of the base aggregate was 5%, it was not possible to achieve this because of the highly permeable nature of the aggregate; the moisture had drained by the time moisture content measurements were made for quality control purposes. Quality control was performed on the base course layer as described above. The average base course density was 2268 kg/m^3 (141.6 lb/ft^3), compared to the modified Proctor maximum dry density of 2383 kg/m^3 (148.8 lb/ft^3). This corresponds to 95% compaction.

Asphalt Paving

The test sections were paved with hot-mixed asphalt concrete by a local contractor according to New Hampshire Department of Transportation specifications. The process began by hand placement of the asphalt near all the edges of the test basin (Fig. 26). The asphalt was subsequently brought in by dump truck and spread with a paver (Fig. 27). The asphalt was placed in a 50-mm (2-in.) base layer, followed by a 50- or 100-mm

Figure 26. Hand placement of asphalt near the north edge of the test basin.

Figure 27. Paving operation during placement of the surface course of asphalt. The dump truck containing the asphalt concrete is in the background, and the paver is shown in the middle.

(2- or 4-in.) surface course (e.g., Fig. 27). The asphalt concrete temperature during placement and compaction was monitored to assure that it was according to NH specifications, between 135°C and 154°C (275-310°F). Compaction was achieved by using a vibratory paving roller (Fig. 28). Nuclear density measurements were made during rolling to ensure proper compaction and air void content (Fig. 28). Thermocouples and pressure cells were embedded in the hot mixed asphalt during paving in the same manner as the εmu gages were (as described above) (Fig. 22). Figure 29 shows the paved test sections and marked test windows.

Figure 28. Steel drum roller compacting the surface of the asphalt concrete layer. Note the nuclear gage in the middle of the image.

Figure 29. Paved test sections and marked test windows. The traffic was applied in the direction away from the viewer; the loading transition zone is in the foreground.

Dynamic Modulus Values of Asphalt

Laboratory-determined dynamic modulus values of the asphalt were required for the modeling effort (i.e., Clapp 2007). Hence, after construction, three 100-mm- (4-in.-) diameter specimens were obtained approximately 0.3 m from the edge of the test basin and shipped to Worcester Polytechnic Institute for determination of dynamic modulus values according to AASHTO TP 62-03. The results are listed in Table 9.

Table 9. Dynamic modulus values of asphalt placed in test basin, determined according to AASHTO TP 62-03.

Temp (°C; °F)	Frequency (Hz)	Stress (kPa; psi)	Dynamic modulus (MPa; ksi)
4.4; 40	25	30.1; 4.37	17160; 2490
	10	32.0; 4.64	15200; 2210
	5	32.4; 4.70	14250; 2067
	1	39.2; 5.69	12770; 1852
	0.5	37.1; 5.38	11490; 1667
	0.1	31.6; 4.58	8742; 1268
21.1; 70	25	Corrupt data	Corrupt data
	10	Corrupt data	Corrupt data
	5	28.1; 4.08	4481; 650
	1	37.3; 5.41	2902; 421
	0.5	36.1; 5.24	2318; 336
	0.1	30.2; 4.38	1495; 217
37.8; 100	25	12.5; 1.81	3675; 533
	10	25.9; 3.76	2670; 387
	5	29.5; 4.28	2077; 301
	1	37.0; 5.37	1129; 164
	0.5	36.4; 5.28	870; 126
	0.1	30.3; 4.40	536; 78

Water Addition to Decrease Subgrade Stiffness

After the test sections were constructed, FWD analyses (described below) indicated that the subgrade stiffness ranged from approximately 109 to 138 MPa (16 to 20 ksi) (Table 10). Water was then added to the subgrade over an extended period to reduce the stiffness to come as close as possible to the original target modulus of approximately 34.5 MPa (5 ksi). A 150-mm (6-in.) width of asphalt was removed from along the sides of the test basin to expose the base layer of crushed rock, and short sections of PVC

tubing were installed in the center of the test basin area to a depth of 50 mm (2 in.) into the subgrade to assure that water addition never resulted in saturation of the base aggregate layer (Fig. 30).

Table 10. Back-calculated modulus values based on FWD tests and the ELMOD program.

Test section	Subgrade modulus (MPa; ksi)		Base modulus (MPa; ksi)	
	12/2/05	5/15/06	12/2/05	5/15/06
1	118.6; 17.2	60.0; 8.7	221.3; 32.1	211.0; 30.6
2	137.9; 20.0	56.5; 8.2	121.4; 17.6	110.3; 16.0
3	108.3; 15.7	54.5; 7.9	335.8; 48.7	281.3; 40.8
4	113.8; 16.5	52.4; 7.6	182.0; 26.4	109.9; 15.9
5	111.0; 16.1	57.2; 8.3	317.9; 46.1	200.6; 29.1
6	133.1; 19.3	60.0; 8.7	261.3; 37.9	188.9; 27.4
7	124.8; 18.1	79.3; 11.5	346.1; 50.2	302.7; 43.9
8	133.1; 19.3	77.9; 11.3	328.2; 47.6	277.2; 40.2

Figure 30. Trench formed by asphalt removal from the edge of the test basin. Water was added to the base layer exposed in the trench to decrease the stiffness of the subgrade layer.

The amount of water required to saturate the subgrade for a thickness of 6 ft was estimated at 47.47 m^3 (5,400 gallons). Water was added in increments of 0.92 m^3 (105 gallons) at a time, with application intervals being at least 48 hours. Water was added with a garden hose (with an attached water meter) along the length of the trenches so that water did not pond at any one location. Water levels were checked in the wells during and

immediately after adding the water to assure that the base did not become saturated by this process. The volumetric soil moisture sensors were monitored with time, and FWD tests were performed periodically on the test sections to obtain back-calculated estimates of the subgrade resilient modulus values. Figure 31 shows the locations of the FWD test points; the numbers on the plan indicate the FWD testing points that are located in the transition zone for the wheel load application in the test section of the same number. The watering procedure was continued until there was a leveling of the water content values in the subgrade and the back-calculated resilient modulus values were relatively constant.

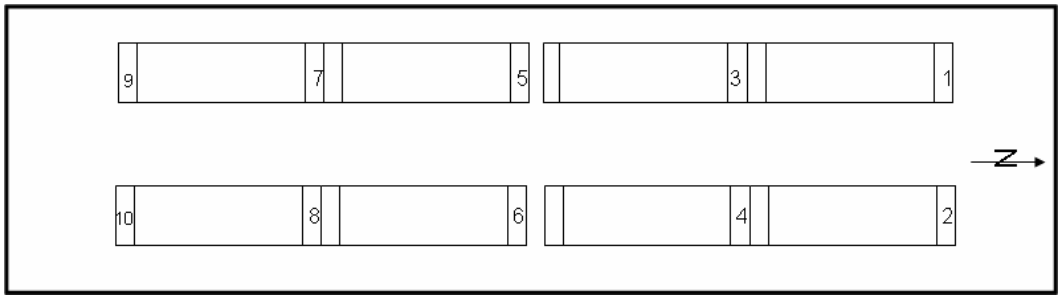

Figure 31. Plan view showing the test area, test sections, and FWD points (labeled 1 through 10). The FWD points 1 through 8 are on the northern transition zone of the test section labeled with the same number.

Table 10 contains the subgrade and base modulus values in December 2005 and May 2006, as measured with the FWD, just prior to testing. The modulus values were back-calculated with the commercially available ELMOD 5 program from Dynatest utilizing the Odemark-Boussinesq method of equivalent thickness in which the outer geophone readings are used to determine the non-linear characteristics of the subgrade and the inner geophones are used to determine the upper pavement layer moduli (Dynatest International 2003). The depth to bedrock was fixed at 2.44 m (96 in.). A fixed pavement modulus value was used, based on laboratory measurements of dynamic modulus value. This was 3584.6 MPa (519.9 ksi) at 21.1°C (70°F), and the measured asphalt temperatures were inserted into the data files (the measured temperature was 18.9°C, or 66°F, on both days).

6 Conclusion

A set of full-scale pavement test sections was constructed and instrumented as a part of a national pooled-fund study to evaluate the reinforcing effect of a geogrid placed between the base and subgrade layers of pavement typically constructed by state transportation agencies. Prior studies reported significant benefits related to the presence of a geogrid layer with soft subgrades and relatively thin asphalt layers compared to typical state highways. The test sections were constructed for this study to help evaluate the potential benefits of geogrid reinforcement in pavement structures representative of modern highways. The testing of the pavement test sections includs accelerated pavement testing by means of a heavy vehicle simulator under controlled temperature and moisture conditions.

Subsequent publications will present the accelerated traffic test results, including the pavement response in terms of stress and strain, and the pavement performance in terms of permanent deformation and other forms of distress observed. Analyses of the test results will provide the basis for the development of pavement models compatible with future modifications to NCHRP 1-37A, *Guide for Mechanistic-Empirical Design of New and Rehabilitated Pavement Structures* (NCHRP 2004), currently available from http://www.trb.org/mepdg/.

References

AASHTO. 1993. *Guide for Design of Pavement Structures*. Washington, DC: American Association of State Highway and Transportation Officials.

AASHTO. 1999. *Standard Test Method for Determining the Resilient Modulus of Soils and Aggregate Materials*. Publication AASHTO-T307. Washington, DC: American Association of State Highway and Transportation Officials.

AASHTO. 2001. *Moisture-Density Relations of Soils Using a (4.55-kg) 10-lb Rammer and an (457-mm) 18-in. Drop (Modified Proctor)*. Publication AASHTO-T180. Washington, DC: American Association of State Highway and Transportation Officials.

ASTM. 2001. *Standard Test Method for Determining Tensile Properties of Geogrids by the Single or Multi-Rib Tensile Method*. Publication ASTM D 6637-01. West Conshohocken, PA: ASTM International.

ASTM. 2004. *Standard Test Method for Density of Soil in Place by the Drive-Cylinder Method*. Publication ASTM D 2937-04. West Conshohocken, PA: ASTM International.

Clapp, J. 2007. Analysis of rutting development in flexible pavements with geogrid reinforced base layers using 3D finite element analysis. Master's Thesis University of Maine-Orono, Orono, ME. 212 p.

Clegg, B. 1986. Correlation with California Bearing Ratio. Newsletter No. 2, July. Jolimont, Western Australia: Clegg, Ltd.

Dynatest International. 2003. Elmod 5.0 Quick Start Manual. Stark, FL: Dynatest International.

Helmstrom, C.L., D.N. Humphrey, and J.M. Labbe. 2006. Performance and effectiveness of a thin pavement section using geogrids and drainage geocomposites in a cold region. NETCR60, NETC Project No. 00-8, Prepared for the New England Transportation Consortium.

Janoo, V., L. Irwin, and R. Haehnel. 2003. *Pavement Subgrade Performance Study: Project Overview*. ERDC/CRREL Technical Report 03-05. Hanover, NH: U.S. Army Engineer Research and Development Center, Cold Regions Research and Engineering Laboratory.

NCHRP. 2004. *Mechanistic-Empirical Design of New and Rehabilitated Pavement Structures*. NCHRP 1-37A. Washington, DC: National Cooperative Highway Research Program. (http://www.trb.org/mepdg/)

Perkins, S.W. 1999. "Mechanical Response of Geosynthetic-Reinforced Flexible Pavements," Geosynthetics International, Vol. 6, No. 5, pp. 347-382.

Perkins, S.W., and E.R. Cortez. 2005. Evaluation of base-reinforced pavements using a heavy vehicle simulator. *Geosynthetics International* 12(2): 86–98.

Perkins, S.W., and M. Ismeik. 1997. A synthesis and evaluation of geosynthetic-reinforced bases in flexible pavements: Part I. *Geosynthetics International* 4(6): 549–604.

Texas Measurements, Inc. 2008. Strain gages. Web page. College Stations, TX: Texas Measurements, Inc. Accessed 2 January 2008. (www.straingage.com/strain_gage/what_strain.php)

Vischer, W. 2003. *Low-Volume Road Flexible Pavement Design with Geogrid-Reinforced Base*. Transportation Research Record 1819. Washington, DC: Transportation Research Board.

Webster, S.L., R.H. Grau, and T.P. Williams. 1992. *Description and Application of Dual Mass Dynamic Cone Penetrometer*. Instruction Report GL-92-3. Vicksburg, MS: U.S. Army Waterways Experimental Station.

Appendix A: Instrumentation Locations in Each Test Section

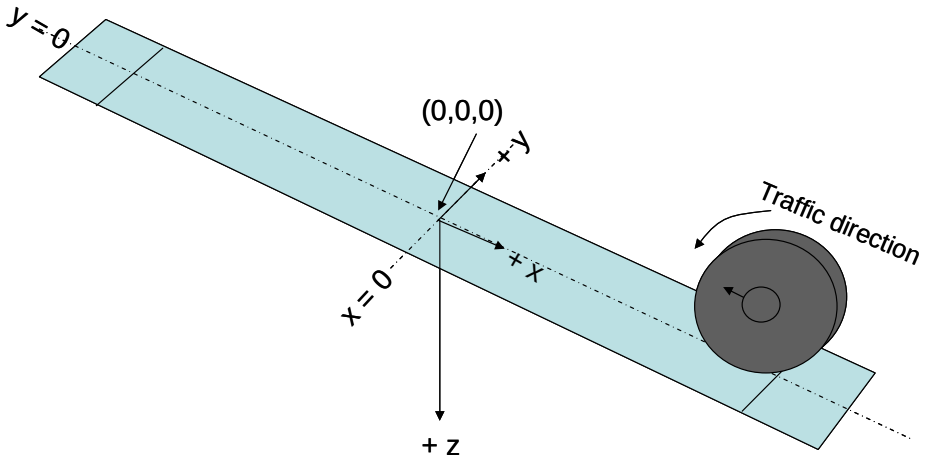

Figure A1. Local coordinate system for each test section.

Table A1 documents the locations of the thermocouples. Test windows are defined as the area where traffic is applied (including wheel wander). Five thermocouples were installed in each test section. Two sensors were located in the subgrade at different depths. One sensor is located in the middle of the base course, one sensor is located in the middle of the asphalt concrete, and one sensor is located in the air 0.91 m (3 ft) above the asphalt surface to monitor the air temperature.

Table A1. Location of thermocouples in the test sections.

Test Section	ID*	Location		
		X (mm; in.)	Y (mm; in.)	Z (mm; in.)
1	W1-T1	2134; 84	0; 0	305; 12
	W1-T2	2134; 84	0; 0	495; 19.5
	W1-T3	2134; 84	0; 0	1295; 51
	W1-T4	2134; 84	0; 0	76; 3
	W1-T5	2134; 84	1981; 78	–914; –36
2	W2-T1	2134; 84	0; 0	254; 10
	W2-T2	2134; 84	0; 0	445; 17.5
	W2-T3	2134; 84	0; 0	1245; 49
	W2-T4	2134; 84	0; 0	51; 2
	W2-T5	2134; 84	–4420; –174	–914; –36
3	W3-T1	2134; 84	0; 0	305; 12
	W3-T2	2134; 84	0; 0	495; 19.5
	W3-T3	2134; 84	0; 0	1295; 51
	W3-T4	2134; 84	0; 0	76; 3
	W3-T5	2134; 84	1981; 78	–914; –36
4	W4-T1	2134; 84	0; 0	305; 12
	W4-T2	2134; 84	0; 0	495; 19.5
	W4-T3	2134; 84	0; 0	1295; 51
	W4-T4	2134; 84	0; 0	76; 3
	W4-T5	2134; 84	–4420; –174	–914; –36
5	W5-T1	2134; 84	0; 0	457; 18
	W5-T2	2134; 84	0; 0	800; 31.5
	W5-T3	2134; 84	0; 0	1295; 51
	W5-T4	2134; 84	0; 0	76; 3
	W5-T5	2134; 84	1981; 78	–914; –36
6	W6-T1	2134; 84	0; 0	406; 16
	W6-T2	2134; 84	0; 0	749; 29.5
	W6-T3	2134; 84	0; 0	1245; 49
	W6-T4	2134; 84	0; 0	76; 3
	W6-T5	2134; 84	–4420; –174	–914; –36
7	W7-T1	2134; 84	0; 0	457; 18
	W7-T2	2134; 84	0; 0	800; 31.5
	W7-T3	2134; 84	0; 0	1295; 51
	W7-T4	2134; 84	0; 0	76; 3
	W7-T5	2134; 84	1981; 78	–914; –36
8	W8-T1	2134; 84	0; 0	406; 16
	W8-T2	2134; 84	0; 0	749; 29.5
	W8-T3	2134; 84	0; 0	1245; 49
	W8-T4	2134; 84	0; 0	76; 3
	W8-T5	2134; 84	–4420; –174	–914; –36

*W = Window; T=Thermocouple

Table A2. Location of moisture sensors in the test sections.

Test Section	ID*	Location		
		X (mm; in.)	Y (mm; in.)	Z (mm; in.)
1	W1-M1	2134; 84	0; 0	305; 12
	W1-M2	2134; 84	0; 0	495; 19.5
	W1-M3	2134; 84	0; 0	1295; 51
2	W2-M1	2134; 84	0; 0	254; 10
	W2-M2	2134; 84	0; 0	445; 17.5
	W2-M3	2134; 84	0; 0	1295; 51
3	W3-M1	2134; 84	0; 0	305; 12
	W3-M2	2134; 84	0; 0	495; 19.5
	W3-M3	2134; 84	0; 0	1295; 51
4	W4-M1	2134; 84	0; 0	254; 10
	W4-M2	2134; 84	0; 0	445; 17.5
	W4-M3	2134; 84	0; 0	1295; 51
5	W5-M1	2134; 84	0; 0	457; 18
	W5-M2	2134; 84	0; 0	800; 31.5
	W5-M3	2134; 84	0; 0	1295; 51
6	W6-M1	2134; 84	0; 0	406; 16
	W6-M2	2134; 84	0; 0	749; 29.5
	W6-M3	2134; 84	0; 0	1295; 51
7	W7-M1	2134; 84	0; 0	457; 18
	W7-M2	2134; 84	0; 0	800; 31.5
	W7-M3	2134; 84	0; 0	1295; 51
8	W8-M1	2134; 84	0; 0	406; 16
	W8-M2	2134; 84	0; 0	749; 29.5
	W8-M3	2134; 84	0; 0	1295; 51

*W = Window; M=Moisture sensor

Table A3. Location of stress sensors in the test sections.

Test Section	ID*	Direction	Location		
			X (mm; in.)	Y (mm; in.)	Z (mm; in.)
1	W1-G11	Vertical	–457; –18	0; 0	229; 9
	W1-G12	Longitudinal	–1067; –42	0; 0	229; 9
	W1-G13	Transverse	–1067; –42	–152; –6	229; 9
	W1-G21	Vertical	–457; –18	0; 0	533; 21
	W1-G22	Longitudinal	–1067; –42	0; 0	533; 21
	W1-G23	Transverse	–1067; –42	–152; –6	533; 21
	W1-G31	Vertical	–457; –18	0; 0	1295; 51
2	W2-G11	Vertical	–457; –18	0; 0	178; 7
	W2-G12	Longitudinal	–1067; –42	0; 0	178; 7
	W2-G13	Transverse	–1067; –42	–152; –6	178; 7
	W2-G21	Vertical	–457; –18	0; 0	483; 19
	W2-G22	Longitudinal	–1067; –42	0; 0	483; 19
	W2-G23	Transverse	–1067; –42	-152; -6	483; 19
	W2-G31	Vertical	–457; –18	0; 0	1245; 49
3	W3-G11	Vertical	–457; –18	0; 0	229; 9
	W3-G12	Longitudinal	–1067; –42	0; 0	229; 9
	W3-G13	Transverse	–1067; –42	–152; –6	229; 9
	W3-G21	Vertical	–457; –18	0; 0	533; 21
	W3-G22	Longitudinal	–1067; –42	0; 0	533; 21
	W3-G23	Transverse	–1067; –42	–152; –6	533; 21
	W3-G31	Vertical	–457; –18	0; 0	1295; 51
4	W4-G11	Vertical	–457; –18	0; 0	178; 7
	W4-G12	Longitudinal	–1067; –42	0; 0	178; 7
	W4-G13	Transverse	–1067; –42	–152; –6	178; 7
	W4-G21	Vertical	–457; –18	0; 0	483; 19
	W4-G22	Longitudinal	–1067; –42	0; 0	483; 19
	W4-G23	Transverse	–1067; –42	–152; –6	483; 19
	W4-G31	Vertical	–457; –18	0; 0	1245; 49
5	W5-G11	Vertical	–457; –18	0; 0	229; 9
	W5-G12	Longitudinal	–1067; –42	0; 0	229; 9
	W5-G13	Transverse	–1067; –42	–152; –6	229; 9
	W5-G21	Vertical	–457; –18	0; 0	838; 33
	W5-G22	Longitudinal	–1067; –42	0; 0	838; 33
	W5-G23	Transverse	–1067; –42	–152; –6	838; 33
	W5-G31	Vertical	–457; –18	0; 0	1295; 51
6	W6-G11	Vertical	–457; –18	0; 0	178; 7
	W6-G12	Longitudinal	–1067; –42	0; 0	178; 7
	W6-G13	Transverse	–1067; –42	–152; –6	178; 7
	W6-G21	Vertical	–457; –18	0; 0	787; 31
	W6-G22	Longitudinal	–1067; –42	0; 0	787; 31
	W6-G23	Transverse	–1067; –42	–152; –6	787; 31
	W6-G31	Vertical	–457; –18	0; 0	1245; 49
7	W7-G11	Vertical	–457; –18	0; 0	229; 9

	W7-G12	Longitudinal	–1067; –42	0; 0	229; 9
	W7-G13	Transverse	–1067; –42	–152; –6	229; 9
	W7-G21	Vertical	–457; –18	0; 0	838; 33
	W7-G22	Longitudinal	–1067; –42	0; 0	838; 33
	W7-G23	Transverse	–1067; –42	–152; –6	838; 33
	W7-G31	Vertical	–457; –18	0; 0	1295; 51
8	W8-G11	Vertical	–457; –18	0; 0	178; 7
	W8-G12	Longitudinal	–1067; –42	0; 0	178; 7
	W8-G13	Transverse	–1067; –42	–152; –6	178; 7
	W8-G21	Vertical	–457; –18	0; 0	787; 31
	W8-G22	Longitudinal	–1067; –42	0; 0	787; 31
	W8-G23	Transverse	–1067; –42	–152; –6	787; 31
	W8-G31	Vertical	–457; –18	0; 0	1245; 49

*W = Window; G=Stress sensor

Table A4. Location of soil and asphalt strain sensors in the test sections.

Test Section	ID*	Direction	Location		
			X (mm; in.)	Y (mm; in.)	Z (mm; in.)
1	W1-E1	Z	457; 18	0; 0	140; 5.5
	W1-E4	Z	457; 18	0; 0	305; 12
	W1-E7	Z	457; 18	0; 0	470; 18.5
	W1-E10	Z	457; 18	0; 0	610; 24
	W1-E13	Z	457; 18	0; 0	762; 30
	W1-E16	Z	457; 18	0; 0	914; 36
	W1-E19	Z	457; 18	0; 0	1067; 42
	W1-E22	Z	457; 18	0; 0	1219; 48
	W1-E23	Z	457; 18	0; 0	1372; 54
	W1-E24	Z	457; 18	0; 0	1524; 60
	W1-E25	Z	457; 18	0; 0	1676; 66
	W1-E2	X	610; 24	0; 0	140; 5.5
	W1-E5	X	610; 24	0; 0	305; 12
	W1-E8	X	610; 24	0; 0	470; 18.5
	W1-E11	X	610; 24	0; 0	610; 24
	W1-E14	X	610; 24	0; 0	762; 30
	W1-E17	X	610; 24	0; 0	914; 36
	W1-E20	X	610; 24	0; 0	1067; 42
	W1-E3	Y	457; 18	152; 6	140; 5.5
	W1-E6	Y	457; 18	152; 6	305; 12
	W1-E9	Y	457; 18	152; 6	470; 18.5
	W1-E12	Y	457; 18	152; 6	610; 24
	W1-E15	Y	457; 18	152; 6	762; 30
	W1-E18	Y	457; 18	152; 6	914; 36
	W1-E21	Y	457; 18	152; 6	1067; 42
	W1-E26	Z	0; 0	0; 0	140; 5.5
	W1-E27	X	152; 6	0; 0	140; 5.5
	W1-E28	Y	0; 0	152; 6	140; 5.5
2	W2-E1	Z	457; 18	0; 0	89; 3.5
	W2-E4	Z	457; 18	0; 0	254; 10
	W2-E7	Z	457; 18	0; 0	419; 16.5
	W2-E10	Z	457; 18	0; 0	559; 22
	W2-E13	Z	457; 18	0; 0	711; 28
	W2-E16	Z	457; 18	0; 0	864; 34
	W2-E19	Z	457; 18	0; 0	1016; 40
	W2-E22	Z	457; 18	0; 0	1168; 46
	W2-E23	Z	457; 18	0; 0	1321; 52
	W2-E24	Z	457; 18	0; 0	1473; 58
	W2-E25	Z	457; 18	0; 0	1626; 64
	W2-E2	X	610; 24	0; 0	89; 3.5
	W2-E5	X	610; 24	0; 0	254; 10
	W2-E8	X	610; 24	0; 0	419; 16.5
	W2-E11	X	610; 24	0; 0	559; 22
	W2-E14	X	610; 24	0; 0	711; 28

	W2-E17	X	610; 24	0; 0	864; 34
	W2-E20	X	610; 24	0; 0	1016; 40
	W2-E3	Y	457; 18	152; 6	89; 3.5
	W2-E6	Y	457; 18	152; 6	254; 10
	W2-E9	Y	457; 18	152; 6	419; 16.5
	W2-E12	Y	457; 18	152; 6	559; 22
	W2-E15	Y	457; 18	152; 6	711; 28
	W2-E18	Y	457; 18	152; 6	864; 34
	W2-E21	Y	457; 18	152; 6	1016; 40
	W2-E26	Z	0; 0	0; 0	89; 3.5
	W2-E27	X	152; 6	0; 0	89; 3.5
	W2-E28	Y	0; 0	152; 6	89; 3.5
3	W3-E1	Z	457; 18	0; 0	140; 5.5
	W3-E4	Z	457; 18	0; 0	305; 12
	W3-E7	Z	457; 18	0; 0	470; 18.5
	W3-E10	Z	457; 18	0; 0	610; 24
	W3-E13	Z	457; 18	0; 0	762; 30
	W3-E16	Z	457; 18	0; 0	914; 36
	W3-E19	Z	457; 18	0; 0	1067; 42
	W3-E22	Z	457; 18	0; 0	1219; 48
	W3-E23	Z	457; 18	0; 0	1372; 54
	W3-E24	Z	457; 18	0; 0	1524; 60
	W3-E25	Z	457; 18	0; 0	1676; 66
	W3-E2	X	610; 24	0; 0	140; 5.5
	W3-E5	X	610; 24	0; 0	305; 12
	W3-E8	X	610; 24	0; 0	470; 18.5
	W3-E11	X	610; 24	0; 0	610; 24
	W3-E14	X	610; 24	0; 0	762; 30
	W3-E17	X	610; 24	0; 0	914; 36
	W3-E20	X	610; 24	0; 0	1067; 42
	W3-E3	Y	457; 18	152; 6	140; 5.5
	W3-E6	Y	457; 18	152; 6	305; 12
	W3-E9	Y	457; 18	152; 6	470; 18.5
	W3-E12	Y	457; 18	152; 6	610; 24
	W3-E15	Y	457; 18	152; 6	762; 30
	W3-E18	Y	457; 18	152; 6	914; 36
	W3-E21	Y	457; 18	152; 6	1067; 42
	W3-E26	Z	0; 0	0; 0	140; 5.5
	W3-E27	X	152; 6	0; 0	140; 5.5
	W3-E28	Y	0; 0	152; 6	140; 5.5
4	W4-E1	Z	457; 18	0; 0	89; 3.5
	W4-E4	Z	457; 18	0; 0	254; 10
	W4-E7	Z	457; 18	0; 0	419; 16.5
	W4-E10	Z	457; 18	0; 0	559; 22
	W4-E13	Z	457; 18	0; 0	711; 28
	W4-E16	Z	457; 18	0; 0	864; 34
	W4-E19	Z	457; 18	0; 0	1016; 40
	W4-E22	Z	457; 18	0; 0	1168; 46

	W4-E23	Z	457; 18	0; 0	1321; 52
	W4-E24	Z	457; 18	0; 0	1473; 58
	W4-E25	Z	457; 18	0; 0	1626; 64
	W4-E2	X	610; 24	0; 0	89; 3.5
	W4-E5	X	610; 24	0; 0	254; 10
	W4-E8	X	610; 24	0; 0	419; 16.5
	W4-E11	X	610; 24	0; 0	559; 22
	W4-E14	X	610; 24	0; 0	711; 28
	W4-E17	X	610; 24	0; 0	864; 34
	W4-E20	X	610; 24	0; 0	1016; 40
	W4-E3	Y	457; 18	152; 6	89; 3.5
	W4-E6	Y	457; 18	152; 6	254; 10
	W4-E9	Y	457; 18	152; 6	419; 16.5
	W4-E12	Y	457; 18	152; 6	559; 22
	W4-E15	Y	457; 18	152; 6	711; 28
	W4-E18	Y	457; 18	152; 6	864; 34
	W4-E21	Y	457; 18	152; 6	1016; 40
	W4-E26	Z	0; 0	0; 0	89; 3.5
	W4-E27	X	152; 6	0; 0	89; 3.5
	W4-E28	Y	0; 0	152; 6	89; 3.5
5	W5-E1	Z	457; 18	0; 0	140; 5.5
	W5-E4	Z	457; 18	0; 0	305; 12
	W5-E7	Z	457; 18	0; 0	470; 18.5
	W5-E10	Z	457; 18	0; 0	610; 24
	W5-E13	Z	457; 18	0; 0	762; 30
	W5-E16	Z	457; 18	0; 0	914; 36
	W5-E19	Z	457; 18	0; 0	1067; 42
	W5-E22	Z	457; 18	0; 0	1219; 48
	W5-E23	Z	457; 18	0; 0	1372; 54
	W5-E24	Z	457; 18	0; 0	1524; 60
	W5-E25	Z	457; 18	0; 0	1676; 66
	W5-E2	X	610; 24	0; 0	140; 5.5
	W5-E5	X	610; 24	0; 0	305; 12
	W5-E8	X	610; 24	0; 0	470; 18.5
	W5-E11	X	610; 24	0; 0	610; 24
	W5-E14	X	610; 24	0; 0	762; 30
	W5-E17	X	610; 24	0; 0	914; 36
	W5-E20	X	610; 24	0; 0	1067; 42
	W5-E3	Y	457; 18	152; 6	140; 5.5
	W5-E6	Y	457; 18	152; 6	305; 12
	W5-E9	Y	457; 18	152; 6	470; 18.5
	W5-E12	Y	457; 18	152; 6	610; 24
	W5-E15	Y	457; 18	152; 6	762; 30
	W5-E18	Y	457; 18	152; 6	914; 36
	W5-E21	Y	457; 18	152; 6	1067; 42
	W5-E26	Z	0; 0	0; 0	140; 5.5
	W5-E27	X	152; 6	0; 0	140; 5.5

	W5-E28	Y	0; 0	152; 6	140; 5.5
6	W6-E1	Z	457; 18	0; 0	89; 3.5
	W6-E4	Z	457; 18	0; 0	254; 10
	W6-E7	Z	457; 18	0; 0	406; 16
	W6-E10	Z	457; 18	0; 0	559; 22
	W6-E13	Z	457; 18	0; 0	724; 28.5
	W6-E16	Z	457; 18	0; 0	864; 34
	W6-E19	Z	457; 18	0; 0	1016; 40
	W6-E22	Z	457; 18	0; 0	1168; 46
	W6-E23	Z	457; 18	0; 0	1321; 52
	W6-E24	Z	457; 18	0; 0	1473; 58
	W6-E25	Z	457; 18	0; 0	1626; 64
	W6-E2	X	610; 24	0; 0	89; 3.5
	W6-E5	X	610; 24	0; 0	254; 10
	W6-E8	X	610; 24	0; 0	406; 16
	W6-E11	X	610; 24	0; 0	559; 22
	W6-E14	X	610; 24	0; 0	724; 28.5
	W6-E17	X	610; 24	0; 0	864; 34
	W6-E20	X	610; 24	0; 0	1016; 40
	W6-E3	Y	457; 18	152; 6	89; 3.5
	W6-E6	Y	457; 18	152; 6	254; 10
	W6-E9	Y	457; 18	152; 6	406; 16
	W6-E12	Y	457; 18	152; 6	559; 22
	W6-E15	Y	457; 18	152; 6	724; 28.5
	W6-E18	Y	457; 18	152; 6	864; 34
	W6-E21	Y	457; 18	152; 6	1016; 40
	W6-E26	Z	0; 0	0; 0	89; 3.5
	W6-E27	X	152; 6	0; 0	89; 3.5
	W6-E28	Y	0; 0	152; 6	89; 3.5
7	W7-E1	Z	457; 18	0; 0	140; 5.5
	W7-E4	Z	457; 18	0; 0	305; 12
	W7-E7	Z	457; 18	0; 0	457;18
	W7-E10	Z	457; 18	0; 0	610; 24
	W7-E13	Z	457; 18	0; 0	775;30.5
	W7-E16	Z	457; 18	0; 0	914; 36
	W7-E19	Z	457; 18	0; 0	1067; 42
	W7-E22	Z	457; 18	0; 0	1219; 48
	W7-E23	Z	457; 18	0; 0	1372; 54
	W7-E24	Z	457; 18	0; 0	1524; 60
	W7-E25	Z	457; 18	0; 0	1676; 66
	W7-E2	X	610; 24	0; 0	140; 5.5
	W7-E5	X	610; 24	0; 0	305; 12
	W7-E8	X	610; 24	0; 0	457;18
	W7-E11	X	610; 24	0; 0	610; 24
	W7-E14	X	610; 24	0; 0	775;30.5
	W7-E17	X	610; 24	0; 0	914; 36
	W7-E20	X	610; 24	0; 0	1067; 42

	W7-E3	Y	457; 18	152; 6	140; 5.5
	W7-E6	Y	457; 18	152; 6	305; 12
	W7-E9	Y	457; 18	152; 6	457;18
	W7-E12	Y	457; 18	152; 6	610; 24
	W7-E15	Y	457; 18	152; 6	775;30.5
	W7-E18	Y	457; 18	152; 6	914; 36
	W7-E21	Y	457; 18	152; 6	1067; 42
	W7-E26	Z	0; 0	0; 0	140; 5.5
	W7-E27	X	152; 6	0; 0	140; 5.5
	W7-E28	Y	0; 0	152; 6	140; 5.5
8	W8-E1	Z	457; 18	0; 0	89; 3.5
	W8-E4	Z	457; 18	0; 0	254; 10
	W8-E7	Z	457; 18	0; 0	406; 16
	W8-E10	Z	457; 18	0; 0	559; 22
	W8-E13	Z	457; 18	0; 0	724; 28.5
	W8-E16	Z	457; 18	0; 0	864; 34
	W8-E19	Z	457; 18	0; 0	1016; 40
	W8-E22	Z	457; 18	0; 0	1168; 46
	W8-E23	Z	457; 18	0; 0	1321; 52
	W8-E24	Z	457; 18	0; 0	1473; 58
	W8-E25	Z	457; 18	0; 0	1626; 64
	W8-E2	X	610; 24	0; 0	89; 3.5
	W8-E5	X	610; 24	0; 0	254; 10
	W8-E8	X	610; 24	0; 0	406; 16
	W8-E11	X	610; 24	0; 0	559; 22
	W8-E14	X	610; 24	0; 0	724; 28.5
	W8-E17	X	610; 24	0; 0	864; 34
	W8-E20	X	610; 24	0; 0	1016; 40
	W8-E3	Y	457; 18	152; 6	89; 3.5
	W8-E6	Y	457; 18	152; 6	254; 10
	W8-E9	Y	457; 18	152; 6	406; 16
	W8-E12	Y	457; 18	152; 6	559; 22
	W8-E15	Y	457; 18	152; 6	724; 28.5
	W8-E18	Y	457; 18	152; 6	864; 34
	W8-E21	Y	457; 18	152; 6	1016; 40
	W8-E26	Z	0; 0	0; 0	89; 3.5
	W8-E27	X	152; 6	0; 0	89; 3.5
	W8-E28	Y	0; 0	152; 6	89; 3.5

*W = Test section (Window); E = εmu sensor

Table A5. Location of geogrid strain gages in the test sections.

Test Section	ID*	Direction	Location		
			X (mm; in.)	Y (mm; in.)	Top; Bottom
3	W3-S1	Transverse	–916; –36	–305; –12	Top
	W3-S2	Transverse	–916; –36	–305; –12	Bottom
	W3-S3	Transverse	–1219; –48	0; 0	Top
	W3-S4	Transverse	–1219; –48	0; 0	Bottom
	W3-S5	Longitudinal	–1524; –60	0; 0	Top
	W3-S6	Longitudinal	–1524; –60	0; 0	Bottom
	W3-S7	Transverse	–1829; –72	0; 0	Top
	W3-S8	Transverse	–1829; –72	0; 0	Bottom
	W3-S9	Transverse	–2134; –84	305; 12	Top
	W3-S10	Transverse	–2134; –84	305; 12	Bottom
4	W4-S1	Transverse	–916; –36	–305; –12	Top
	W4-S2	Transverse	–916; –36	–305; –12	Bottom
	W4-S3	Transverse	–1219; –48	0; 0	Top
	W4-S4	Transverse	–1219; –48	0; 0	Bottom
	W4-S5	Longitudinal	–1524; –60	0; 0	Top
	W4-S6	Longitudinal	–1524; –60	0; 0	Bottom
	W4-S7	Transverse	–1829; –72	0; 0	Top
	W4-S8	Transverse	–1829; –72	0; 0	Bottom
	W4-S9	Transverse	–2134; –84	305; 12	Top
	W4-S10	Transverse	–2134; –84	305; 12	Bottom
7	W7-S1	Transverse	–916; –36	–305; –12	Top
	W7-S2	Transverse	–916; –36	–305; –12	Bottom
	W7-S3	Transverse	–1219; –48	0; 0	Top
	W7-S4	Transverse	–1219; –48	0; 0	Bottom
	W7-S5	Longitudinal	–1524; –60	0; 0	Top
	W7-S6	Longitudinal	–1524; –60	0; 0	Bottom
	W7-S7	Transverse	–1829; –72	0; 0	Top
	W7-S8	Transverse	–1829; –72	0; 0	Bottom
	W7-S9	Transverse	–2134; –84	305; 12	Top
	W7-S10	Transverse	–2134; –84	305; 12	Bottom
8	W8-S1	Transverse	–916; –36	–305; –12	Top
	W8-S2	Transverse	–916; –36	–305; –12	Bottom
	W8-S3	Transverse	–1219; –48	0; 0	Top
	W8-S4	Transverse	–1219; –48	0; 0	Bottom
	W8-S5	Longitudinal	–1524; –60	0; 0	Top
	W8-S6	Longitudinal	–1524; –60	0; 0	Bottom
	W8-S7	Transverse	–1829; –72	0; 0	Top
	W8-S8	Transverse	–1829; –72	0; 0	Bottom
	W8-S9	Transverse	–2134; –84	305; 12	Top
	W8-S10	Transverse	–2134; –84	305; 12	Bottom

* W = Window; S = Strain gage

Appendix B: As-Built Subgrade and Base Course Moisture Determined with Troxler Nuclear Gage

Tables B1 and B2 document the gravimetric moisture content measured with the Troxler nuclear gage in the west and east "lanes" of the test basin, respectively, while B3 and B4 document the dry density determinations of the west and east lanes. In the west lane (Test Sections 1, 3, 5, and 7), readings were taken along a line that was 0.3 m (1 ft) from the west edge of the traffic window. In the east lane, the line was only 0.15 m (0.5 ft) from the west edge of the traffic window. North readings were taken in the traffic window right at the line of transition where the full load is first applied. Middle readings were taken in the middle of the test window. South readings were taken in the traffic window right at the line of transition where the full load is first removed (Fig. B1).

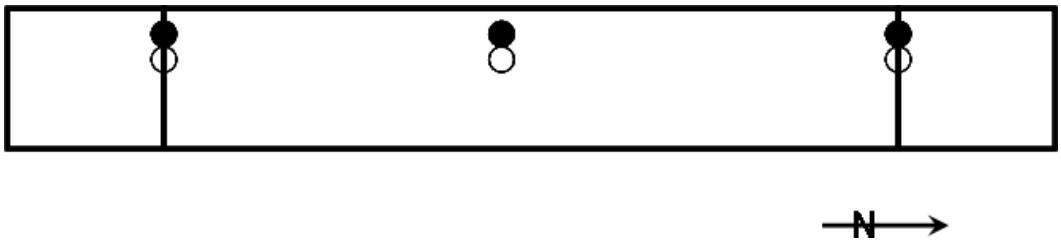

Figure B1. Plan view showing the locations of Troxler nuclear gage readings with respect to the traffic window of each test section (not to scale). The traffic load is fully applied in the center portion of the window, and the two marked ends are the transition zones. The empty circles represent the reading locations for Test Sections 1, 3, 5, and 7, and the dark circles represent Test Sections 2, 4, 6, and 8.

Table B1. Base and subgrade gravimetric moisture content in Test Sections 1, 3, 5, and 7, determined with the nuclear gage.

Location	Depth (in.*)	Test Section 1			Test Section 3			Test Section 5			Test Section 7		
		North	Middle	South	North	Middle	South	North	Middle	South	North	Middle	South
Top of base	7	2.7	2.6	2.9	3.2	3.0	3.0	3.2	3.4	3.0	2.8	3.1	2.4
Base course	10	2.7	2.7	3.2	3.8	3.1	3.5	3.8	4.3	3.1	2.4	2.8	2.3
Base course	16-20							2.8	2.6	2.8	2.4	3.1	3.3
Base course	19							1.9	2.1	2.0	2.4	2.2	2.3
Subgrade	16-20	10.2	11.4	10.3	10.1	10.8	12.2						
Subgrade	25-30	12.3	12.0	12.9	12.0	11.7	12.4	11.3	11.6	10.9	11.6	10.8	10.1
Subgrade	31	12.8	12.4	13.1	13.3	13.0	12.7	12.8	13.2	13.3	12.8	12.1	12.5
Subgrade	37	12.9	12.3	11.3	12.4	11.9	12.4	12.2	12.4	12.6	12.8	12.0	12.0
Subgrade	43	11.8	11.9	11.6	13.1	12.9	11.4	12.7	12.5	11.0	11.7	11.0	9.7
Lower subgrade	117	13.6	6.2	11.0	8.9	10.0	8.5	9.3	8.6	14.5	10.2	8.1	12.4

1 inch = 2.54 cm.

Table B2. Base and subgrade gravimetric moisture content in Test Sections 2, 4, 6, and 8, determined with the nuclear gage.

Location	Depth (in.)	Test Section 2			Test Section 4			Test Section 6			Test Section 8		
		North	Middle	South	North	Middle	South	North	Middle	South	North	Middle	South
Top of base	7	2.5	2.9	2.8	2.6	2.9	2.6	2.8	3.4	2.8	3.0	3.5	3.0
Base course	10	2.3	2.1	2.4	2.0	2.6	2.9	2.9	2.8	2.7	2.9	3.7	4.7
Base course	16-20							2.1	3.4	3.1	3.1	3.3	2.5
Base course	19							2.2	2.5	2.5	2.3	2.1	2.0
Subgrade	16-20	12.5	12.4	12.4	11.7	12.0	12.4						
Subgrade	25-30	12.4	12.6	12.6	12.0	12.4	13.1	11.1	11.0	11.4	11.7	11.5	10.3
Subgrade	31	13.3	13.9	12.2	13.7	12.9	13.9	12.6	12.4	12.7	12.9	13.1	13.4
Subgrade	37	12.4	12.1	11.4	11.8	12.6	11.8	11.7	11.6	10.7	11.9	11.0	11.5
Subgrade	43	12.0	12.4	11.9	11.2	11.8	11.6	12.2	11.6	10.6	12.5	13.1	11.1
Lower subgrade	117	8.5	9.1	10.2	9.3	10.0	12.2	7.0	6.0	4.1	9.5	8.6	8.7

Table B3. Base and subgrade density (kg/m³; pcf) in Test Sections 1, 3, 5, and 7, determined with the nuclear gage.

Location	Depth (in.*)	Test Section 1			Test Section 3			Test Section 5			Test Section 7		
		North	Middle	South	North	Middle	South	North	Middle	South	North	Middle	South
Top of base	7	2353; 146.9	2361; 147.4	2430; 151.7	2281; 142.4	2294; 143.2	2272; 141.8	2262; 141.2	2198; 137.2	2353; 146.9	2336; 145.8	2320; 144.8	2268; 141.6
Base course	10	2219; 138.5	2193; 136.9	2120; 132.9	2216; 138.3	2150; 134.2	2244; 140.1	2185; 136.1	2111; 131.8	2172; 135.6	2357; 147.1	2308; 144.1	2244; 140.1
Base course	16-20							2264; 141.3	2262; 141.2	2336; 145.8	2278; 142.2	2299; 143.5	2328; 145.3
Base course	19							2162; 135.0	2041; 127.4	2251; 140.5	2353; 146.9	2256; 140.8	2275; 142.0
Subgrade	16-20	1826; 114.0	1826; 114.0	1862; 116.2	1850; 115.5	1834; 114.5	1831; 114.3						
Subgrade	25-30	1884; 117.6	1873; 116.9	1890; 118.0	1862; 116.2	1911; 119.3	1882; 117.5	1897; 118.4	1911; 119.3	1894; 118.2	1889; 117.9	1913; 119.4	1858; 116.0
Subgrade	31	1847; 115.3	1849; 115.4	1852; 115.6	1858; 116.0	1882; 117.5	1886; 117.7	1876; 117.1	1826; 114.0	1828; 114.1	1868; 116.6	1882; 117.5	1884; 117.6
Subgrade	37	1829; 114.2	1852; 115.6	1882; 117.5	1858; 116.0	1863; 116.3	1849; 115.4	1854; 115.7	1870; 116.7	1846; 115.2	1858; 116.0	1862; 116.2	1829; 114.2
Subgrade	43	1834; 114.5	1876; 117.1	1837; 114.7	1815; 113.3	1846; 115.2	1879; 117.3	1829; 114.2	1879; 117.3	1863; 116.3	1860; 116.1	1764; 110.1	1802; 112.5
Lower subgrade	117	1849; 115.4	1765; 110.2	1783; 111.3	1661; 103.	1658; 103.5	1653; 103.2	1674; 104.4	1684; 105.1	1650; 103.0	1778; 111.0	1703; 106.3	1650; 103.0

Table B4. Base and subgrade density (kg/m³; pcf) in Test Sections 2, 4, 6, and 8, determined with the nuclear gage.

Location	Depth (in.)	Test Section 2			Test Section 4			Test Section 6			Test Section 8		
		North	Middle	South	North	Middle	South	North	Middle	South	North	Middle	South
Top of base	7	2288; 142.8	2337; 145.9	2316; 144.6	2342; 146.2	2400; 149.8	2288; 142.8	2352; 146.8	2382; 148.7	2316; 144.6	2310; 144.2	2334; 145.7	2272; 141.8
Base course	10	2224; 138.8	2143; 133.8	2225; 138.9	2185; 136.4	2272; 141.8	2302; 143.7	2230; 139.2	2195; 137.0	2230; 139.2	2344; 146.3	2337; 145.9	2318; 144.7
Base course	16-20							2262; 141.2	2344; 146.3	2308; 144.1	2280; 142.3	2278; 142.2	2333; 145.6
Base course	19							2033; 126.9	2214; 138.2	2357; 147.1	2240; 139.8	2339; 146.0	2325; 145.1
Subgrade	16-20	1850; 115.5	1833; 114.4	1828; 114.1	1829; 114.2	1829; 114.2	1831; 114.3						
Subgrade	25-30	1826; 114.0	1919; 11938	1889; 117.9	1929; 120.4	1895; 118.3	1826; 114.0	1882; 117.5	1970; 123.0	1919; 119.8	1910; 119.2	1826; 114.0	1850; 115.5
Subgrade	31	1878; 117.2	1876; 117.1	1860; 116.1	1829; 114.2	1837; 114.7	1828; 114.1	1846; 115.2	1833; 114.4	1884; 117.6	1863; 116.3	1839; 114.8	1828; 114.1
Subgrade	37	1873; 116.9	1826; 114.0	1844; 115.1	1863; 116.3	1844; 114.7	1913; 119.4	1831; 114.3	1898; 118.5	1913; 119.4	1868; 116.6	1927; 120.3	1882; 117.5
Subgrade	43	1873; 116.9	1846; 115.2	1882; 117.5	1839; 114.8	1862; 115.1	1849; 115.4	1849; 115.4	1754; 109.5	1725; 107.7	1868; 116.6	1831; 114.3	1820; 113.6
Lower subgrade	117	1661; 103.7	1729; 107.9	1607; 100.3	1695; 105.8	1645; 102.7	1596; 99.6	1773; 110.7	1852; 115.6	1812; 113.1	1666; 104.0	1684; 105.1	1656; 103.4

Appendix C: CBR Determinations at the Top of the Finished Subgrade Determined according to Dynamic Cone Penetrometer and Clegg Impact Hammer Measurements

For each test section, dynamic cone penetrometer (DCP) measurements were made at three locations at approximately the center of a longitudinal line through the test window. North, Middle, and South refers to the transition lines (north and south) and center of the test window as shown in Figure B1. The following relation was used to provide the estimates shown in Table C1 (Webster et al. 1992):

$$CBR(\%) = \frac{292}{\left(\frac{mm}{blow}\right)^{1.12}}. \quad \text{(A1)}$$

Raw DCP data used to make the determinations in Table C1 is provided in Table C2.

Table C1. CBR estimates, based on DCP tests.

Test Section	Depth* (mm; in.)	CBR		
		North	Middle	South
1	0/ 0	10	14	11
	305/ 12	22	37	36
	610/ 24	26	24	24
	914/ 36	12	12	12
2	0/ 0	12	14	10
	305/ 12	36	37	40
	610/ 24	38	28	38
	914/ 36	14	19	11
3	0/ 0	11	13	9
	305/ 12	36	44	43
	610/ 24	24	25	20
	914/ 36	12	19	11
4	0/ 0	10	13	12
	305/ 12	40	43	36
	610/ 24	38	30	36
	914/ 36	11	24	24
5	0/ 0	12	22	9
	305/ 12	26	17	43
	610/ 24	18	14	20
	914/ 36	16	37	11
6	0/ 0	16	27	15
	305/ 12	36	37	32
	610/ 24	26	22	26
	914/ 36	14	10	9
7	0/ 0	16	22	18
	305/ 12	26	22	22
	610/ 24	22	14	20
	914/ 36	18	27	20
8	0/ 0	12	25	16
	305/ 12	34	39	32
	610/ 24	24	19	26
	914/ 36	26	38	30

* Depth was measured from top of subgrade.

Table C2. DCP readings used to determine the CBR estimates shown in Table C1.

Test Window	North		Middle		South	
	Number of blows	Accumulative penetration (mm)	Number of blows	Accumulative penetration (mm)	Number of blows	Accumulative penetration (mm)
1	0	11	0	5	0	6
	1	40	1	30	1	45
	2	83	2	74	1	68
	3	138	2	108	2	100
	7	200	2	137	2	130
	4	232	2	160	2	158
	6	275	3	186	2	182
	3	300	3	215	4	210
	5	324	2	235	3	235
	5	345	3	265	4	265
	7	385	2	285	3	291
	5	420	3	304	4	318
	4	452	4	329	5	340
	4	482	4	354	6	366
	4	505	4	384	5	401
	4	525	4	420	4	428
	4	550	4	461	4	450
	4	572	3	482	6	480
	4	602	3	501	6	511
	4	628	3	521	6	555
	4	655	4	552	4	591
	4	675	4	586	4	638
	4	691	4	623	4	677
	6	718	4	670	4	705
	4	742	2	687	4	732
	4	771	2	699	6	765
	4	812	3	717	6	803
	1	825	4	738	4	828
	2	853	3	756	4	865
	2	891	4	783	6	930
	1	915	4	818	0	6
	1	942	3	849	1	45
	0	11	3	890	1	68
	1	40	2	923	2	100
	2	83	0	5	2	130
	3	138	1	30	2	158
	7	200	2	74	2	182
	4	232	2	108	4	210
	6	275	2	137	3	235
	3	300	2	160	4	265
	5	324	3	186	3	291
	5	345	3	215	4	318
	7	385	2	235	5	340
	5	420	3	265	6	366
	4	452	2	285	5	401
			3	304	4	428
			4	329		
2	0	10	0	7	0	5
	1	45	1	48	1	42
	1	66	1	70	1	64

	1	85	2	101	1	83
	2	114	2	131	2	118
	2	137	2	154	2	143
	2	160	2	177	2	176
	2	182	2	203	2	201
	4	221	2	223	2	228
	3	240	2	239	2	245
	4	264	2	251	2	263
	4	292	4	275	5	292
	4	317	3	293	5	325
	4	346	7	337	5	357
	4	370	6	355	5	383
	4	392	6	378	5	412
	6	415	6	397	5	444
	5	439	6	418	4	465
	7	470	6	450	4	489
	4	497	6	481	4	508
	4	522	6	507	4	522
	7	560	6	532	6	556
	4	583	6	558	6	583
	4	608	6	593	6	633
	4	645	4	625	4	676
	4	695	4	662	4	733
	4	751	4	695	4	782
	3	769	4	718	3	799
	5	795	4	738	3	814
	7	832	4	760	4	830
	4	854	6	789	5	858
	2	873	4	815	5	893
	3	896	4	845	2	914
	2	918	4	885		
			3	919		
3	0	6	0	7	0	7
	1	49	1	36	1	58
	1	76	1	55	1	85
	1	96	1	74	1	106
	2	127	2	110	1	121
	2	155	2	142	2	145
	2	180	3	172	2	165
	3	209	4	200	2	183
	3	230	4	227	2	203
	3	251	4	255	2	220
	4	280	4	278	4	248
	4	311	5	305	4	271
	4	337	4	327	4	293
	5	367	4	352	5	318
	5	397	4	378	5	345
	5	428	5	409	4	366
	5	457	5	433	5	388

	7	489	5	460	5	413
	5	518	5	492	5	442
	4	553	5	527	5	474
	5	600	5	570	5	511
	3	636	3	597	5	558
	2	661	3	635	5	613
	3	692	3	674	3	661
	3	722	3	701	3	687
	3	744	3	725	3	703
	3	762	3	742	4	723
	5	793	4	768	3	744
	5	828	4	793	3	764
	3	855	4	826	5	804
	3	885	3	855	3	837
	5	921	2	878	2	863
			2	892	1	876
			2	927	1	890
					1	905
					1	924
4	0	4	0	4	0	10
	1	36	1	39	1	51
	2	72	1	67	1	76
	2	105	1	86	1	97
	2	133	1	102	2	132
	2	160	2	135	2	158
	2	186	2	164	3	188
	2	217	2	193	3	206
	2	236	2	221	3	227
	2	258	2	247	3	251
	3	280	2	265	4	228
	6	312	4	288	4	298
	4	336	4	310	4	322
	5	365	6	340	4	344
	5	392	6	365	6	377
	5	417	6	392	6	415
	5	439	6	420	5	447
	5	463	6	452	7	468
	10	510	6	483	7	504
	7	533	6	509	7	539
	7	562	6	536	7	588
	7	595	6	573	3	625
	7	638	6	619	3	658
	7	695	6	682	3	684
	7	758	4	718	3	703
	5	781	4	742	5	728
	5	804	4	765	5	757
	7	833	4	788	5	777
	7	867	4	812	5	815
	5	906	4	837	5	856

			5	877	5	907
			3	906	3	953
			2	925		
5	0	4	0	4	0	10
	1	36	1	39	1	51
	2	72	1	67	1	76
	2	105	1	86	1	97
	2	133	1	102	2	132
	2	160	2	135	2	158
	2	186	2	164	3	188
	2	217	2	193	3	206
	2	236	2	221	3	227
	2	258	2	247	3	251
	3	280	2	265	4	228
	6	312	4	288	4	298
	4	336	4	310	4	322
	5	365	6	340	4	344
	5	392	6	365	6	377
	5	417	6	392	6	415
	5	439	6	420	5	447
	5	463	6	452	7	468
	10	510	6	483	7	504
	7	533	6	509	7	539
	7	562	6	536	7	588
	7	595	6	573	3	625
	7	638	6	619	3	658
	7	695	6	682	3	684
	7	758	4	718	3	703
	5	781	4	742	5	728
	5	804	4	765	5	757
	7	833	4	788	5	777
	7	867	4	812	5	815
	5	906	4	837	5	856
			5	877	5	907
			3	906	3	953
			2	925		
6	0	0	0	0	0	0
	2	35	2	35	1	25
	3	65	3	65	3	55
	4	98	3	90	3	80
	3	125	3	115	3	105
	2	150	3	140	4	135
	2	175	3	170	4	170
	3	200	3	200	4	210
	5	230	3	225	3	240
	5	255	4	250	3	265
	5	280	5	275	5	290
	4	305	5	300	5	320
	3	330	4	325	5	345

	3	355	3	350	5	370
	3	385	3	375	6	395
	3	410	3	400	5	420
	4	435	4	450	5	445
	4	460	5	480	4	470
	5	485	4	505	4	500
	5	510	4	530	3	525
	5	540	4	560	3	555
	4	570	3	585	3	590
	4	605	3	615	3	630
	4	650	2	640	2	660
	2	675	2	670	2	695
	2	705	2	702	2	735
	2	735	2	740	2	780
	2	770	2	775	1	805
	2	810	2	810	1	830
	1	835	2	850	1	855
	1	865	1	875	1	880
	1	895	2	915	3	905
	1	925			3	930
7	0	5	0	10	0	5
	1	30	2	35	1	30
	2	55	4	70	2	55
	2	80	3	96	2	80
	2	110	3	125	2	105
	2	135	3	155	2	135
	2	165	3	185	3	175
	2	190	3	210	2	202
	5	225	4	240	5	233
	6	250	4	275	5	260
	4	280	3	305	4	290
	4	310	2	330	3	315
	4	335	3	365	3	345
	5	360	3	395	3	370
	4	385	3	420	3	395
	4	415	4	450	4	423
	3	445	3	475	4	450
	3	480	4	505	4	480
	1	505	3	535	4	505
	2	535	2	560	4	533
	2	565	1	585	4	565
	2	605	2	615	3	590
	1	630	2	650	2	615
	1	660	2	685	3	650
	1	695	2	723	2	680
	1	720	2	755	2	710
	1	750	3	785	2	735
	2	790	4	815	3	765
	3	815	4	840	5	790

	8	840	4	865	6	815
	7	865	5	890	8	845
	9	890	3	915	5	870
	7	915			5	895
					5	920
8	0	0	0	5	0	10
	2	35	2	40	3	40
	2	60	2	70	4	70
	3	90	3	95	4	100
	4	120	3	123	3	130
	3	145	3	150	3	160
	3	175	3	180	3	190
	3	205	2	205	4	215
	3	235	3	235	3	238
	4	264	5	265	4	265
	5	290	5	290	4	290
	5	315	5	320	3	315
	4	340	4	350	3	343
	5	370	3	375	3	370
	4	395	4	400	3	400
	6	420	4	428	4	425
	6	445	4	445	4	450
	6	470	4	480	4	475
	5	500	4	505	5	500
	4	525	4	535	5	525
	3	550	4	568	4	550
	3	580	3	600	5	580
	3	615	3	635	5	610
	2	640	3	665	3	635
	2	670	2	700	3	660
	2	710	2	740	3	688
	2	750	2	790	3	715
	1	780	1	815	4	740
	1	805	2	853	5	765
	1	830	2	878	8	790
	2	860	4	905	8	820
	3	890	4	930	8	845
	4	915			9	870
					9	898
					14	925

The Clegg impact hammer is a 4.5-kg (10-lb) hammer that is raised to a height of 457 mm (18 in.) inside a guide tube and then dropped. A hand-held meter measures the peak deceleration as the hammer hits the surface. The deceleration is reported in tens of gravities; this unit is called Clegg Impact Value (CIV). The percent CBR is determined from the following equation (Clegg 1986):

$$CBR(\%) = \left[0.24\left(CIV\right)+1\right]^2 . \quad \text{(C1)}$$

For each test section, the percent CBR estimates obtained in this way at a location near the north end of the traffic window, at the middle, and near the south end of the traffic window are presented in Table C3. Three drops were measured at each point, and the average of the three values was recorded.

Table C3. Clegg CBR on the test sections.

Test Section	Location	Drop 1	Drop 2	Drop 3	Average
1	North	12	15	15	14
	Middle	13	23	21	19
	South	9	12	13	11
2	North	10	15	15	13
	Middle	6	10	12	9
	South	10	13	15	13
3	North	9	12	12	10
	Middle	13	17	19	16
	South	5	7	10	7
4	North	10	13	15	13
	Middle	10	13	15	13
	South	6	9	12	9
5	North	15	23	23	20
	Middle	17	28	34	26
	South	23	36	36	32
6	North	15	23	26	21
	Middle	13	19	19	17
	South	15	23	26	21
7	North	13	21	21	18
	Middle	19	26	28	24
	South	26	43	43	36
8	North	15	19	19	18
	Middle	13	19	19	17
	South	12	21	26	19

REPORT DOCUMENTATION PAGE

Form Approved
OMB No. 0704-0188

Public reporting burden for this collection of information is estimated to average 1 hour per response, including the time for reviewing instructions, searching existing data sources, gathering and maintaining the data needed, and completing and reviewing this collection of information. Send comments regarding this burden estimate or any other aspect of this collection of information, including suggestions for reducing this burden to Department of Defense, Washington Headquarters Services, Directorate for Information Operations and Reports (0704-0188), 1215 Jefferson Davis Highway, Suite 1204, Arlington, VA 22202-4302. Respondents should be aware that notwithstanding any other provision of law, no person shall be subject to any penalty for failing to comply with a collection of information if it does not display a currently valid OMB control number. **PLEASE DO NOT RETURN YOUR FORM TO THE ABOVE ADDRESS.**

1. REPORT DATE *(DD-MM-YYYY)*	**2. REPORT TYPE**	**3. DATES COVERED** *(From - To)*
April 2008	Technical Report	

4. TITLE AND SUBTITLE

Construction and Instrumentation of Full-Scale Geogrid Reinforced Pavement Test Sections

5a. CONTRACT NUMBER

5b. GRANT NUMBER

5c. PROGRAM ELEMENT NUMBER

6. AUTHOR(S)

Karen S. Henry, Edel R. Cortez, Lawrence S. Danyluk,
Gregory Brentrup, Nathan Lamie, and Troy W. Arnold

5d. PROJECT NUMBER

5e. TASK NUMBER

5f. WORK UNIT NUMBER

7. PERFORMING ORGANIZATION NAME(S) AND ADDRESS(ES)

U.S. Army Engineer Research and Development Center
Cold Regions Research and Engineering Laboratory
72 Lyme Road
Hanover, NH 03755-1290

8. PERFORMING ORGANIZATION REPORT NUMBER

ERDC/CRREL TR-08-6

9. SPONSORING / MONITORING AGENCY NAME(S) AND ADDRESS(ES)

Federal Highway Administration

10. SPONSOR/MONITOR'S ACRONYM(S)

11. SPONSOR/MONITOR'S REPORT NUMBER(S)

12. DISTRIBUTION / AVAILABILITY STATEMENT

Approved for public release; distribution is unlimited.

Available from NTIS, Springfield, Virginia 22161.

13. SUPPLEMENTARY NOTES

14. ABSTRACT

A study is being conducted on full-scale pavement test sections to assess geogrid base reinforcement in flexible pavements representative of major highways. This report documents the construction and instrumentation of those test sections. The design of the test sections was based on a pavement design life of 3×10^6 equivalent single axle loads. There are two asphalt concrete and two base course thicknesses. One test section at each asphalt and base thickness was constructed with geogrid reinforcement and one without geogrid. The geogrid is located at the base course/subgrade interface. Test sections are instrumented to measure stress, strain, moisture, and temperature. They were constructed in the Frost Effects Research Facility with moisture and temperature control. The subgrade soil is AASHTO A-4 (USCS ML), and the as-built subgrade modulus values, determined by falling weight deflectometer, ranged from approximately 55.2 to 75.8 MPa (8-11 ksi). A concrete floor (simulating natural bedrock) is 2.44 m (8 ft) below the pavement surface. Analyses of results generated by this project will provide evaluation of geogrid reinforcement and will serve as the basis for the development of pavement models compatible with NCHRP 1-37A, Guide for Mechanistic-Empirical Design of New and Rehabilitated Pavement Structures (available from http://www.trb.org/mepdg/).

15. SUBJECT TERMS

Pavements
Flexible pavements
Geogrid

16. SECURITY CLASSIFICATION OF:			**17. LIMITATION OF ABSTRACT**	**18. NUMBER OF PAGES**	**19a. NAME OF RESPONSIBLE PERSON**
a. REPORT	**b. ABSTRACT**	**c. THIS PAGE**			**19b. TELEPHONE NUMBER** *(include area code)*
U	U	U	U	71	